Computers and Operations Research 113 (2020) 104776

Contents lists available at ScienceDirect

Computers and Operations Research

journal homepage: www.elsevier.com/locate/cor

Optimal charging facility location and capacity for electric vehicles considering route choice and charging time equilibrium

Rui Chen[a,c,1], Xinwu Qian[b,1], Lixin Miao[c,d], Satish V. Ukkusuri[b,*]

[a] Department of Industrial Engineering, Tsinghua University, Beijing 100084, China
[b] Lyles School of Civil Engineering, Purdue Univeristy, 550 Stadium Mall Drive, West Lafayette, IN 47907, USA
[c] Division of Logistics and Transportation, Graduate School at Shenzhen, Tsinghua University, Shenzhen 518055, China
[d] Intelligent Transportation and Logistics Systems Laboratory, Tsinghua-Berkeley Shenzhen Institute, Shenzhen 518055, China

ARTICLE INFO

Article history:
Received 14 September 2018
Revised 6 August 2019
Accepted 20 August 2019
Available online 23 August 2019

Keywords:
Electric vehicle
Facilities location
Waiting time
Charging and route choice equilibrium

ABSTRACT

In this study, the optimal design of location and capacity of charging facilities for electric vehicles (EVs) is investigated. A bi-level mathematical model is proposed to derive optimal design considering the equilibrium of route choice and waiting time for charging. The objective is to minimize the joint cost of facility constructions and EV drivers' travel and waiting time over the network. The upper-level model allocates the facilities and their capacity, while the lower-level model characterizes equilibrium behavior of drivers' route and charging facility choices. In particular, we model drivers at each charging facility as the M(t)/M/n queue and approximate the average queuing time and probability of waiting time as functions of facility capacity and demand arrival rate. The bi-level model is then converted into a single-level model, and the solution algorithm is proposed for iteratively solving the relaxed problems. Comprehensive experiments are conducted on three networks to evaluate algorithm performances, assess solution robustness and understand the scalability of the solution approach on large networks.

1. Introduction

Gasoline for vehicles is the principal petroleum product. Until September 2008, practically all of the existing surplus capacity in major oil-producing regions was consumed by rampant demand growth, leaving the global market more vulnerable to potential petroleum supply disruptions (Huntington, 2010). Electric vehicles (EVs), a promising solution for reducing vehicle emissions and petroleum dependence (Riemann et al., 2015), convert 59–62% of electrical energy to driving power without producing tailpipe pollutants, while conventional vehicles only utilize 17–21% of the energy stored in gasoline (Agrawal et al., 2016). Despite EVs being highly efficient, they account for less than 1% of total vehicles in most countries (Lévay et al., 2017). According to the previous literature, the reasons are manifold but primarily referring to drivers' anxiety over EVs' range and the limited coverage of existing charging facilities (Egbue and Long, 2012). Studies have shown that, if a publicly available and compatible EV charging network exists, potential EV market share could grow up to 5.5 times faster (Dong et al., 2014). These motivate us to investigate the joint optimization of charging facility locations and the capacity of each charging station and contribute to facilitating the adoption of EVs.

1.1. Literature review

Charging facility location problems for EVs seek the optimal placement of charging facilities to minimize construction and transportation costs, while considering other factors. With the development of charging technology and the growing popularity of EVs, we have witnessed the rapid growth of literature in related fields. Early works focused on maximizing demand coverage with a given set of charging facilities (Frade et al., 2011). He et al. (2016) compared three classic facility location models of those and found that the p-median solutions are more effective than the set covering and maximal covering location models when the charging stations are closer to the communities with higher EV demand, but those approaches may not be effective without considering network structures and changes in demand patterns after the construction. Worley et al. (2012) embedded vehicle routing into the charging facility location problem and formulated the problem as a discrete integer programming problem. This makes the solution more adaptive to real life, but the features considered are quite limited. In order to characterize various features on charging facility location problems, more and more effort has been

* Corresponding author.
E-mail address: sukkusur@purdue.edu (S.V. Ukkusuri).
[1] The first two authors contribute equally to the study.

https://doi.org/10.1016/j.cor.2019.104776
0305-0548/

put into the formulation of multi-period planning, flow allocation, stochastic factors and/or other considerations. As those activities appear after the location or construction of the charging facilities, it becomes much more natural to model these features as bi-level or multi-level programs. Jung et al. (2014) introduced a facility location model for locating electric taxi charging stations considering itinerary-interception and solved it with a bi-level simulation-optimization method. Wu and Sioshansi (2017) proposed a bi-level stochastic flow-capturing model optimally to locate fast-charging stations. To provide drivers some information, Gagarin and Corcoran (2018a) investigated the charging station location problem based on reachability graphs while the impact of station capacity and charging demand were neglected. However, without considering the user equilibrium (UE) choice of drivers, the solutions may not be applied as expected because each individual aims to maximize his/her own profit instead of cooperating to achieve the system optimum. To model drivers' responses to the location of charging facilities, He et al. (2014) introduced EV flow dependency on energy consumption and recharging time, and characterized equilibrium behavior of EV drivers over metropolitan road networks. In their study, EV drivers were assumed to determine routes and recharging plans to minimize their travel cost without running out of power. Riemann et al. (2015) developed a model to locate wireless charging facilities to serve maximal traffic flow on a network, where stochastic UE was introduced to capture route-choice behavior of EV drivers. Chen et al. (2016) proposed a new model to describe the equilibrium flow distribution over a road network with charging lanes. In their model, EV drivers' choices of routes and recharging plans dictate which lane to use, how long to charge and at what speed to operate EVs.

The main UE features of the existing studies on the location problem for EVs are summarized in Table 1. It shows that the existing studies mainly focus on the travel time of EVs and little attention has been paid to the waiting time at charging facilities. However, even with the latest charging technology, EV charging time is still significantly higher than gas refueling (20–30 min for a full charge (Sadeghi-Barzani et al., 2014)). This provides major challenges to EVs' usage (Gagarin and Corcoran, 2018b). Therefore, waiting time at charging facilities creates another bottleneck, in addition to the limited coverage of charging facilities. One way to reduce waiting time for EV drivers is through battery swapping technology (Kang et al., 2016), which has fostered related studies on planning for deployment of battery swapping infrastructure. Mak et al. (2013) proposed robust optimization models to study technology advancements on the optimal infrastructure deployment strategy. Widrick et al. (2016) modeled battery charging and discharging operations with various non-stationary characteristics at battery swapping stations. Xu et al. characterized the UE for mixed driver groups with road grade constraints. Table 2 summarizes the main features of the existing studies on the location problem for battery swapping infrastructure. However, without standardized charging protocols, different EV manufacturers (e.g., Tesla and Nissan) have their own battery configurations (Muller, 2013), and it is not cost-effective to supply a variety of batteries at swapping stations. Alternatively, a more promising approach is optimally to design the capacity along with locating charging facilities. This motivates us to study the location of charging facilities with capacity design, which may contribute to a wider acceptance of EVs by the public.

Finally, We are aware of similar studies on the charging facility location problem for EVs in car-sharing literature (e.g. Brandstätter et al., 2017). Boyac et al. proposed an integrated multi-objective mixed integer linear programming model and discrete event simulation framework to optimize operational decisions for vehicle and personnel relocation in a carsharing system with reservations (Boyac et al., 2017). He et al.introduced a mixed

Table 1
Main UE features of the existing studies on charging facility location for EVs.

Study	Problem setting	Model	Solution algorithm	Test examples
He et al. (2013)	UE with route choice & social welfare	Mathematical program with complementarity constraints	CONOPT	Sioux Falls
Jiang and Xie (2014)	UE with mode & route choice	Convex model for mixed equilibrium traffic networks	FW-MLS; PG-PLS	Nguyen-Dupuis; Sioux Falls; Anaheim
He et al. (2014)	UE with route choice & recharging plans	Nonlinear complementarity problem	CONOPT; CPLEX 12.2	Sioux Falls
Riemann et al. (2015)	Stochastic UE with route choice	Mixed-integer nonlinear program	CPLEX 12.6	Nguyen-Dupuis
Chen et al. (2016)	UE with route choice & flow distribution	Mathematical program with complementarity constraints	Active-set	Nguyen-Dupuis; Sioux Falls
Liu and Wang (2017)	UE with route & ownership choice	Tri-level programming	SRAMB	Nguyen-Dupuis; Sioux Falls

* MLS: modified label-setting algorithm.
PLS: preprocessing and label-setting algorithm.
SRAMB: surface response approximation model based solution algorithm.

Table 2
Main features of the existing studies on location for battery swapping infrastructure.

Study	Problem setting	Model	Solution algorithm	Test examples
Yang and Sun (2015)	Location-routing problem	integer programming under various scenarios	SIGALNS; TS-MCWS	NEO classic CVRP data
Mak et al. (2013)	Planning based on a robust optimization framework	Mixed-integer nonlinear program	MISOCPs; CPLEX 12.1	Major freeway network of the San Francisco Bay Area
Widrick et al. (2016)	charging operations with non-stationary characteristics	Finite-horizon, discrete-time Markov decision problem	Dynamic programming	Data from 2013 in the Capital Region, New York
Xu et al. (2017)	UE with road grade constraints	Nonlinear minimization model	Frank-Wolfe algorithm	NguyenDupius; Sioux Falls; YangBell

* SIGALNS: a four-phase heuristic.
TS-MCWS: a two-phase Tabu Search-modified Clarke and Wright Savings heuristic.
MISOCPs: mixed-integer second-order cone programs.

integer second-order cone program to approximate the planning problem faced by service providers of electric vehicle sharing systems in designing a geographical service region (He et al., 2017). These studies provide strategic advice for our problems with parameter settings and sensitivity analysis.

1.2. Contribution

In this study, we seek to address the optimal capacity and location problem of charging facilities for EVs by explicitly modeling queuing time at charging facilities and equilibrium response of EV drivers to travel time and waiting time. We formulate the problem as a bi-level optimization problem, with the upper-level objective being to minimize the joint cost of construction and drivers' travel time and waiting time. The lower-level problem captures equilibrium responses of EV drivers to the upper-level decisions. It is more natural to adopt the bi-level optimization method to tackle location problems considering UE as the UE problem is a non-cooperative game (Friesz et al., 1993; Friesz, 1985). Moreover, we conduct numerical experiments to compare our solution algorithm with the ubiquitous heuristics in location problems to illustrate the superiority of our algorithm on this proposed model. The contributions of our study can be summarized as follows:

1. We propose the first work to optimize both the location and capacity of charging facilities by considering the equilibrium responses of drivers to travel time and waiting time.
2. EVs at each charging facility are modeled as the $M(t)/M/n$ queue, and approximation approaches are then developed, which accurately characterize the average waiting time and waiting probability.
3. The problem is formulated as a mathematical program with complementarity constraints (MPCC), and the solution algorithm is developed, which solves the original problem as a sequence of relaxed nonlinear programming problems.
4. Numerical experiments are conducted on test networks of various sizes to discuss the parameter settings related to the solution algorithms and the robustness of the solutions.

The rest of the paper is organized as follows. The mathematical model is presented in Section 2 with the assumptions and modeling components. Section 3 presents the approximation of the waiting time and the single-level formulation of our problem. Section 4 discusses the nonlinear programming reformulation and the solution algorithm. Section 5 delivers the numerical experiments, and major findings of the study are summarized in Section 6.

2. Mathematical model

2.1. Assumptions

The following assumptions are made in this study to model the EV charging facility location and capacity design problem:

1. We consider a mixed traffic environment, where there are both EVs and gasoline vehicles (GVs), and all EVs and GVs are assumed to be homogeneous.
2. We consider the travel range of EVs being L, i.e., all EVs need to charge after traversing a fixed distance L.
3. There would be at most one facility located on each link.
4. The EV demand is satisfied if all EVs of the OD pair can complete the trip without running out of energy.
5. OD demand is described as the arrival rate of each OD pair, and we assume arrivals at each origin follow a Poisson process.
6. The charging service time follows an exponential distribution.

Table 3
Table of notations.

Sets	
$\mathcal{G}$	network $\mathcal{G} = (\mathcal{N}, \mathcal{A})$ consisting of sets of nodes $\mathcal{N}$ and links $\mathcal{A}$
$\mathcal{N}$	set of all nodes n in network
$\mathcal{A}$	set of all links a in network
$\mathcal{O}$	set of all origin nodes o, where $\mathcal{O} \subseteq \mathcal{N}$
$\mathcal{D}$	set of all origin nodes d, where $\mathcal{D} \subseteq \mathcal{N}$
$\mathcal{W}$	set of all OD pairs w
$\mathcal{R}^w$	set of all feasible routes r of OD pair $w \in \mathcal{W}$
$\mathcal{K}$	set of all candidate facility locations
$\Psi^{w,r}$	set of candidate facility locations capable of recharging EV flows so that the EV can traverse the route r
Φ_k	set of routes with candidate facility location k on them
$\mathcal{T}$	set of all link free flow travel times t_a, $a \in \mathcal{A}$
$\mathcal{C}$	set of all link capacity c_a, $a \in \mathcal{A}$
Parameters	
$\delta_a^{w,r}$	indicator variable that maps trip flow on route r of OD pair w to link a
D_e^w	EV travel demand of OD pair w
D_g^w	GV travel demand of OD pair w
$s_k^{\max}$	maximal capacity of facility k
C_k^1	monetary cost of charging facility k
C_k^2	monetary cost of unit capacity at charging facility k
C^3	monetary cost of travel and waiting time
η	market penetration for electric vehicles
t_a	free flow travel time on link a
c_a	capacity of link a
Decision variables	
x_k	binary variable, 1 if there is a charging facility at location k, 0 otherwise
s_k	designed charging facility capacity at location k
$\lambda_{e,k}^{w,r}$	EV flow variable (arrival rate) on route r between OD pair $w \in \mathcal{W}$, captured by facility k
$\lambda_g^{w,r}$	GV flow variable (arrival rate) on route r between OD pair $w \in \mathcal{W}$
$t_{e,k}^{w,r}$	the cost to EV drivers consists of the trip time along the chosen route r and the waiting time at the selected charging facility k
$t_g^{w,r}$	the cost to GV drivers consists of the trip time along the chosen route r
h_a	flow on link a
T_a	travel time on link a
$\bar{W}_k$	average waiting time at facility k

2.2. Notation

The mathematical notations used in the paper are listed in Table 3.

2.3. Probability of waiting time

Based on assumption 6, the waiting time at each charging facility can be modeled as the $M(t)/M/n$ queuing system with intensity function $\lambda_k(t)$ and service rate μ_k. The probability that waiting time $\Gamma(t)$ is greater than $\bar{t}$ can be written as (Green and Soares, 2007):

$$P(\Gamma(t) > \bar{t}) = \sum_{n=s_k}^{+\infty} \sum_{i=0}^{n-s_k} \frac{\alpha_k{}^i e^{-\alpha_k}}{i!} p_n(t) < p \tag{1}$$

Eq. (1) is used to constrain excessive waiting at any of the constructed facilities, where s_k is the capacity of facility k, p is a constraint for the level of service and $\alpha_k = \mu_k s_k \bar{t}$. $p_n(t)$ is the periodic steady-state probability that n drivers are in the system at time t and is obtained by numerically solving the following set of differential equations (Green et al., 2001):

$$\begin{cases} p_0'(t) = -\lambda(t) p_0(t) + \mu p_1(t) \\ p_n'(t) = \lambda(t) p_{n-1}(t) + (n+1)\mu p_{n+1}(t) - (\lambda(t) + n\mu) p_n(t), \quad 1 \le n < s(t) \\ p_n'(t) = \lambda(t) p_{n-1}(t) + s(t)\mu p_{n+1}(t) - (\lambda(t) + s(t)\mu) p_n(t), \quad n \ge s(t) \end{cases} \tag{2}$$

Thus, $p_n(t)$ is dependent on $s(t)$, which is the charging facility capacity at time t. Let $p_n(t) = g_n(s(t), \lambda(t))$. In this study, we consider the average situation over time $\bar{p}_{k,n} = g_{k,n}(s_k, \lambda_k)$, where $\lambda_k = \lambda_{e,k} = \sum_{(w,r)\in\Phi_k} \lambda_{e,k}^{w,r}$. Let $\bar{P}_{k,n} = \sum_{i=0}^{n} \bar{p}_{k,i}$, which is the probability that the system has fewer than or equal to n drivers on average. Considering the probability that the system has more than n drivers (i.e., $1 - \bar{P}_{k,n}$) increases with increasing λ_k and decreases with increasing s_k, we have:

$$\frac{\partial \bar{P}_{k,n}}{\partial s_k} \ge 0 \tag{3}$$

$$\frac{\partial \bar{P}_{k,n}}{\partial \lambda_k} \le 0 \tag{4}$$

2.4. Choice of drivers

For a given OD pair w, drivers have equal access to all routes in $\mathcal{R}^w$ and all facilities along each route. Consequently, the cost to drivers consists of the trip time along the chosen route and the waiting time at the selected charging facility, which can be expressed as:

$$t_{e,k}^{w,r} = \bar{W}_k(\lambda_{e,k}, s_k) + \sum_{a\in\mathcal{A}} \delta_a^{w,r} T_a(t_a, c_a, h_a) \tag{5}$$

$$t_g^{w,r} = \sum_{a\in\mathcal{A}} \delta_a^{w,r} T_a(t_a, c_a, h_a) \tag{6}$$

where $\delta_a^{w,r}$ is the indicator variable that maps trip flow on route r of OD pair w to link a. $\bar{W}$ is the average waiting time function, and T is the Bureau of Public Roads (BPR) function (Dafermos and

Sparrow, 1969):

$$T_a(t_a, c_a, h_a) = t_a\left(1 + 0.15\left(\frac{h_a}{c_a}\right)^4\right) \tag{7}$$

where t_a is the free flow travel time, and c_a and $h_a = \sum_{w\in\mathcal{W}}\sum_{r\in\mathcal{R}^w}\delta_a^{w,r}(\lambda_g^{w,r} + \sum_{k\in\Psi^{w,r}}\lambda_{e,k}^{w,r})$ are the capacity and flow on link a, respectively.

2.5. Model formulation

We next introduce the definition of charging and route choice equilibrium (CRC Equilibrium).

Definition 1 (CRC Equilibrium)**.** The cost of the trip to each traveler consists of the time on the route that he or she chooses and the charging time at the facility visited. The system is said to reach CRC Equilibrium if no individual traveler can reduce his or her travel cost (travel time and charging time) by unilaterally changing his or her route and charing facility choice.

With the introduction of waiting time and drivers' choice, the problem can be formulated as the following bi-level mixed integer nonlinear programming.

2.5.1. Upper level formulation

$$\text{Minimize } \sum_{k\in\mathcal{K}}(C_k^1 x_k + C_k^2 s_k) + C^3\sum_{w\in\mathcal{W}}\sum_{r\in\mathcal{R}^w}\left(\lambda_g^{w,r}t_g^{w,r} + \sum_{k\in\Psi^{w,r}}\lambda_{e,k}^{w,r}t_{e,k}^{w,r}\right) \tag{8}$$

$$\text{Subject to: } 0 \le s_k \le s_k^{\max}x_k, \forall k \in \mathcal{K} \tag{9}$$

$$x_k \in \{0,1\}, \forall k \in \mathcal{K} \tag{10}$$

$$\sum_{n=s_k}^{\infty}\sum_{i=0}^{n-s_k}\frac{\alpha_k^i e^{-\alpha_k}}{i!}g_{k,n}(s_k, \lambda_{e,k}) \le p, \quad \forall k \in \mathcal{K} \tag{11}$$

The objective function minimizes the joint cost of infrastructure construction, travel time and waiting time. Constraint (9) restricts capacity assignments to constructed facilities. Constraint (10) reflects the binary nature of facility location decisions. Constraint (11) sets the upper bound for the level of service at each charging facility.

2.5.2. Lower level formulation

$$\text{Minimize } \sum_{k\in\mathcal{K}}\int_0^{\lambda_{e,k}}\bar{W}_k(z_1, s_k)dz_1 + \sum_{a\in\mathcal{A}}\int_0^{h_a}T_a(t_a, c_a, z_2)dz_2 \tag{12}$$

$$\text{Subject to: } \lambda_{e,k} = \sum_{(w,r)\in\Phi_k}\lambda_{e,k}^{w,r}, \forall k \in \mathcal{K} \tag{13}$$

$$h_a = \sum_{w\in\mathcal{W}}\sum_{r\in\mathcal{R}^w}\delta_a^{w,r}\left(\lambda_g^{w,r} + \sum_{k\in\Psi^{w,r}}\lambda_{e,k}^{w,r}\right) \tag{14}$$

$$D_e^w = \sum_{r\in\mathcal{R}^w}\sum_{k\in\Psi^{w,r}}\lambda_{e,k}^{w,r}, \forall w \in \mathcal{W} \tag{15}$$

$$D_g^w = \sum_{r\in\mathcal{R}^w}\lambda_g^{w,r}, \forall w \in \mathcal{W} \tag{16}$$

$$0 \le \lambda_{e,k}^{w,r} \le D_e^w x_k, 0 \le \lambda_g^{w,r}, \quad \forall w \in \mathcal{W},\ r \in \mathcal{R}^w,\ k \in \mathcal{K} \tag{17}$$

The objective function (12) minimizes total travel and waiting time over the network, and the derivative, with respect to $\lambda_{e,k}^{w,r}$ and $\lambda_g^{w,r}$, reflects the greedy behavior of users in choosing route and charging facilities. Constraints (13)–(16) ensure flow conservation for each charging facility, link and OD pair. Constraint (17) restricts flow assignments to only constructed facilities. For cleaner representation, we define the feasible region as $\mathcal{H}(x, s) = \{\lambda | Constraints(11), (13) - (17)\}$.

3. Model reformulation

3.1. Waiting time approximation

One difficulty associated with our model arises from Eq. (11), which requires solving the system of differential equations over time and is computationally expensive. More importantly, this prevents us from solving the bi-level programming problem via single-level reformulation. This is because the system of differential equations can only be solved numerically and does not have an analytical closed form solution. As a consequence, the first effort we made to solve the problem was to relax the calculation of waiting time at charging facility by approximating the solution using functions with more suitable mathematical properties.

Define

$$G_k(s_k, \lambda_k) = \sum_{n=s_k}^{+\infty}\sum_{i=0}^{n-s_k}\frac{{\alpha_k}^i e^{-\alpha_k}}{i!}\bar{p}_{k,n} = \sum_{j=0}^{+\infty}\frac{{\alpha_k}^j e^{-\alpha_k}}{j!}P_{k,j} \tag{18}$$

we have:

$$\frac{\partial P_{k,j}}{\partial s_k} = -\frac{\partial \bar{P}_{k,j}}{\partial s_k} \le 0 \tag{19}$$

$$\frac{\partial P_{k,j}}{\partial \lambda_k} = -\frac{\partial \bar{P}_{k,j}}{\partial \lambda_k} \ge 0 \tag{20}$$

where $P_{k,j} = 1 - \bar{P}_{k,j} = \bar{p}_{k,j+s_k} + \bar{p}_{k,j+s_k+1} + \ldots + \bar{p}_{k,\infty}$ for $j = 0, 1, \ldots$ and $1 \ge P_{k,0} \ge P_{k,1} \ge \ldots \ge P_{k,\infty} \ge 0$.

Proposition 1. *$G_k(s_k, \lambda_k)$ has the following properties:*

$$\frac{\partial G_k(s_k, \lambda_k)}{\partial s_k} \le 0 \tag{21}$$

$$\frac{\partial G_k(s_k, \lambda_k)}{\partial \lambda_k} \ge 0 \tag{22}$$

that is, $G_k(s_k, \lambda_k)$ is non-increasing with the increase of s_k and is non-decreasing with the increase of λ_k.

To approximate $G_k(s_k, \lambda_k)$, we conduct Monte-Carlo simulation to generate waiting time and corresponding probability from the M(t)/M/n (distribution of arrival rate is given as in Fig. 1) queuing system with parameters μ, $\bar{t}$ and p. We propose the following two functions, which have consistent mathematical properties with $G_k(s_k, \lambda_k)$ as shown in Proposition 1:

$$G_k^1(s_k, \lambda_k) = \beta_0 + \beta_1 s_k + \beta_2\lambda_k, \quad \beta_1 < 0,\ \beta_2 > 0, \text{for each } k \in \mathcal{K}. \tag{23}$$

$$G_k^2(s_k, \lambda_k) = \beta_0(s_k)^{\beta_1}(\lambda_k)^{\beta_2}, \quad \beta_0 > 0,\ \beta_1 < 0, \beta_2 > 0, \text{ for each } k \in \mathcal{K}. \tag{24}$$

The Least Squares Regression (LSR) is introduced to fit the simulation data to the proposed functions, and an example of fitting results are presented in Table 4 and Fig. 2.

It can be observed that both functions fit the data quite well, with the function G^1 of linear combination form having higher R^2

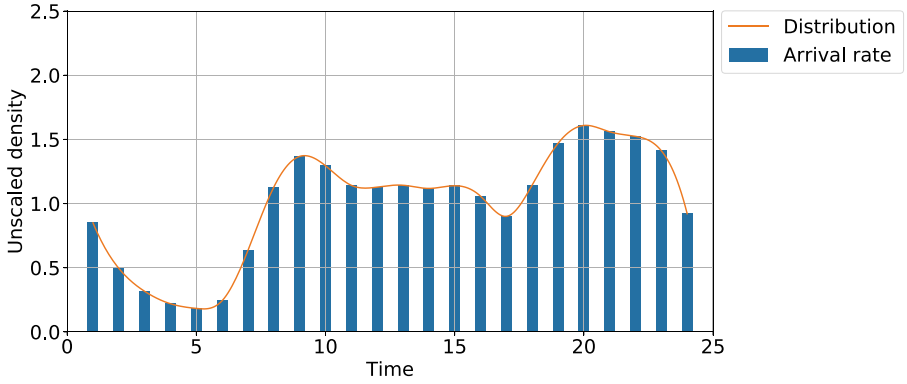

Fig. 1. Distribution of arrival rate.

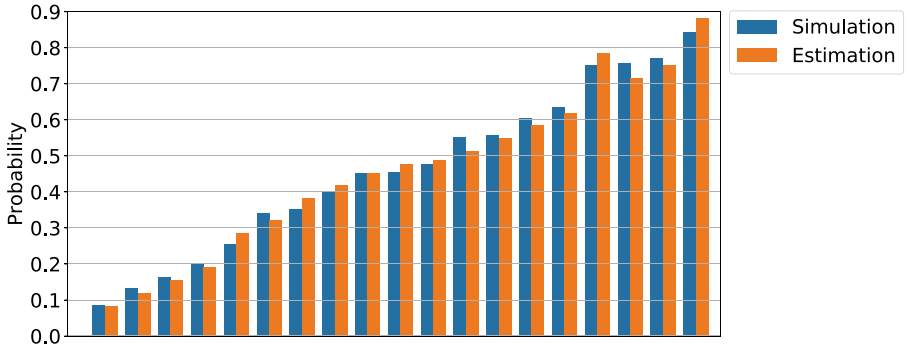

Fig. 2. Estimation of waiting time probability.

Table 4
LSR for waiting time probability constraints (with $\mu = 0.05$, $\bar{t} = 20$, $p = 0.5$).

	regression coefficients				
G	β_0	β_1	β_2	R^2	p value
G^1	0.6178	−0.2081	6.6456	0.9447	<0.01
G^2	22.4832	−6.8171	6.2692	0.8753	<0.01

Table 5
LSR for waiting time constraints (with $\mu = 0.05, \bar{t} = 20, p = 0.5$).

	regression coefficients				
$\bar{W}$	γ_0	γ_1	γ_2	R^2	p value
$\bar{W}^1$	11.8590	−2.0589	77.9135	0.4420	>0.05
$\bar{W}^2$	10.2443	8.1217	1.0000	0.9697	<0.01

* regression coefficients of $\bar{W}^2$ shown here are for some specific s, and R^2 is the average value.

value, meaning that it may explain more variability of the waiting time and fit the data better. Similar results are observed for other sets of parameters, and we therefore choose G^1 as the approximated probability function of waiting time in this study.

For $\bar{W}_k$, its value depends on the flow and capacity at facility k, and intuitively, the average waiting time should be non-decreasing with increasing flow and non-increasing with increasing capacity. Therefore, two candidate function forms are proposed as follows:

$$\bar{W}_k^1(\lambda_k, s_k) = \gamma_0 + \gamma_1 s_k + \gamma_2 \lambda_k, \quad \text{for each } k \in \mathcal{K}. \tag{25}$$

$$\bar{W}_k^2(\lambda_k, s_k) = \gamma_0 \left(\frac{\lambda_k}{\gamma_2}\right)^{\gamma_1(s_k)}, \quad \text{for each } k \in \mathcal{K}. \tag{26}$$

where $\gamma_1(s_k)$ increases with increasing s_k and we again apply the LSR to fit the data with the models, and the results of the same parameter setting are presented in Table 5 and Fig. 3 (different capacities in each subplot):

Being different from G, the average waiting time function is observed to be better approximated by the power function form, with R^2 being significantly higher than the linear combination form, and the fitness is as good as that of the probability function. It is understandable why this happened according to the average waiting time function form of M/M/n queue. As a consequence, we use function $\bar{W}_k^2$ to approximate the average waiting time.

3.2. Single-level reformulation

With the approximation functions for the probability function and average waiting time function, the bi-level programming can now be rewritten as the single-level problem by representing the CRC equilibrium of lower-level problem as complementarity conditions. The single-level reformulation can therefore be written as a MPCC:

$$\text{Minimize} \quad \sum_{k\in\mathcal{K}}(C_k^1 x_k + C_k^2 s_k) + C^3 \sum_{w\in\mathcal{W}} \sum_{r\in\mathcal{R}^w} \left(\lambda_g^{w,r} t_g^{w,r} + \sum_{k\in\Psi^{w,r}} \lambda_{e,k}^{w,r} t_{e,k}^{w,r}\right) \tag{27}$$

$$\text{Subject to:} \quad 0 \le s_k \le s_k^{\max} x_k, \forall k \in \mathcal{K} \tag{28}$$

$$x_k \in \{0, 1\}, \forall k \in \mathcal{K} \tag{29}$$

$$\lambda \in SOL(CP(\mathcal{H}(x, s), F)) \tag{30}$$

with the solution set of $CP(\mathcal{H}(x, s), F)$ being:

$$\begin{aligned} 0 \le \lambda \quad & \perp F(\lambda, x, s) + \nabla_\lambda H(\lambda)^T \mu - \nabla_\lambda C(\lambda, x, s)^T \pi \ge 0 \\ & H(\lambda) = 0 \\ 0 \le \pi \quad & \perp C(\lambda, s, x) \ge 0 \end{aligned} \tag{31}$$

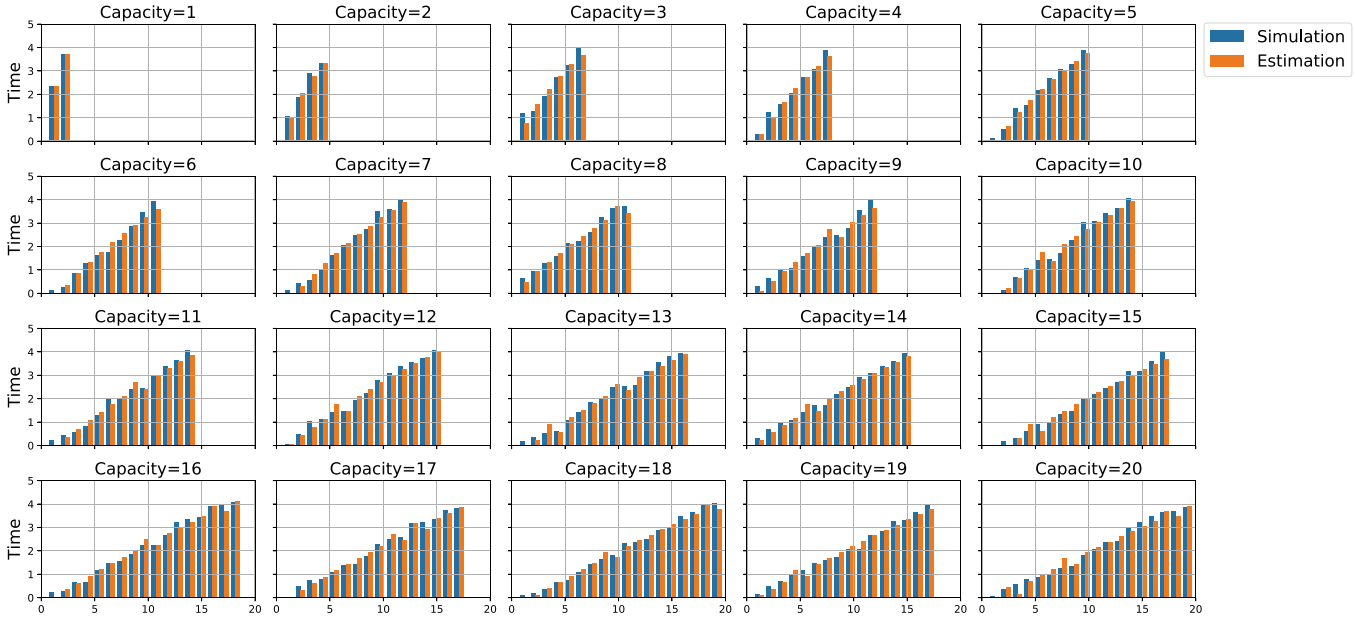

Fig. 3. Estimation of average logarithmic waiting time.

where λ is the vector of route-facility flow $\{\lambda_{e,k}^{w,r} | x_k = 1\} \cup \left\{\lambda_g^{w,r}\right\}$ and $F(\lambda, x, s)$ is the vector of cost function for each route-facility flow variable, where each $F_{e,k}^{w,r}$ and $F_g^{w,r}$ can be expressed as:

$$F_{e,k}^{w,r}(\lambda, x, s) = \bar{W}_k^2\left(\sum_{w,r}\lambda_{e,k}^{w,r}, s_k\right) + \sum_{a\in\mathcal{A}}\delta_a^{w,r}T_a\left(t_a, c_a, \sum_{w,r}\delta_a^{w,r}\left(\lambda_g^{w,r} + \sum_{k\in\Psi^{w,r}}\lambda_{e,k}^{w,r}\right)\right) \tag{32}$$

$$F_g^{w,r}(\lambda, x, s) = \sum_{a\in\mathcal{A}}\delta_a^{w,r}T_a\left(t_a, c_a, \sum_{w,r}\delta_a^{w,r}\left(\lambda_g^{w,r} + \sum_{k\in\Psi^{w,r}}\lambda_{e,k}^{w,r}\right)\right) \tag{33}$$

which is simply the summation of all link travel time on route r and the average waiting time at facility k.

In addition, $H(\lambda) = 0$ is the set of equality constraints as shown in Eq. (15) and (16) for flow conservation, and $C(\lambda, x, s) \geq 0$ is the collection of inequality constraints as shown in Eqs. (11)–(17).

Proposition 2. *The MPCC (27)–(30) has at least one optimal solution if the feasible set is not empty.*

4. Solution approach

4.1. Nonlinear programming formulation

One attractive approach to solve the MPCC (27)–(30) is to reformulate it as a nonlinear programming (NLP) model and solve it using standard NLP solvers. The only difficulty arises from the fact that x_k is a binary variable. Since it is the constraint of the original upper-level problem, we may rewrite the integer constraint as an equivalent complementarity constraint following:

$$x_k(1 - x_k) \leq 0, \quad 0 \leq x_k \leq 1, \forall k \in \mathcal{K} \tag{34}$$

where binary variables are relaxed as continuous variables. We can therefore rewrite the MPCC as an equivalent NLP following:

$$\begin{aligned}
\text{Minimize} \quad & \sum_{k\in\mathcal{K}}\left(C_k^1 x_k + C_k^2 s_k\right) + C^3\sum_{w\in\mathcal{W}}\sum_{r\in\mathcal{R}^w}\left(\lambda_g^{w,r}t_g^{w,r} + \sum_{k\in\Psi^{w,r}}\lambda_{e,k}^{w,r}t_{e,k}^{w,r}\right) \\
\text{Subject to:} \quad & 0 \leq s_k \leq s_k^{\max}x_k, \forall k \in \mathcal{K} \\
& x_k(1 - x_k) \leq 0, \quad 0 \leq x_k \leq 1, \quad \forall k \in \mathcal{K} \\
& (F(\lambda, x, s) + \nabla_\lambda H(\lambda)^T\mu - \nabla_\lambda C(\lambda, x, s)^T\pi)^T\lambda \leq 0 \\
& \lambda \geq 0 \\
& F(\lambda, x, s) + \nabla_\lambda H(\lambda)^T\mu - \nabla_\lambda C(\lambda, x, s)^T\pi \geq 0 \\
& H(\lambda) = 0 \\
& C(\lambda, s, x)^T\pi \leq 0 \\
& \pi \geq 0 \\
& C(\lambda, s, x) \geq 0
\end{aligned} \tag{35}$$

4.2. Algorithm for stationary points

Unfortunately, directly solving the NLP (35) using NLP solvers is likely to fail and be numerically unsafe. This is because the NLP violates the Mangasarian–Fromovitz constraint qualification (MFCQ) at any feasible point (Scheel and Scholtes, 2000), which implies that the KKT multipliers of the NLP are unbounded, and there does not exist any central path and the active constraint normals are linearly dependent. These violate the fundamental requirements for most NLP solution algorithms and introduce numerical challenges to NLP solvers (see examples in Fletcher et al., 2006), and it is known that the complementarity constraints in the NLP are the contributing factors (Leyffer and Munson, 2010).

To avoid this issue, recent efforts (Ban et al., 2006; Dirkse et al., 2002) have shown that the component relaxation of the complementarity condition into a relaxed NLP can help solve MPCC reliably. The main idea is to relax the complementarity constraints by a component τ as:

$$\begin{aligned}
& \textstyle\sum_{k\in\mathcal{K}} x_k(1 - x_k) \leq \tau \\
& (F(\lambda, x, s) + \nabla_\lambda H(\lambda)^T\mu - \nabla_\lambda C(\lambda, x, s)^T\pi)^T\lambda \leq \tau \\
& C(\lambda, s, x)^T\pi \leq \tau
\end{aligned} \tag{36}$$

We name the NLP (35) with the relaxed constraints (36) as $NLP(\tau)$. The MFCQ will therefore hold for $NLP(\tau)$ when $\tau > 0$, and we can

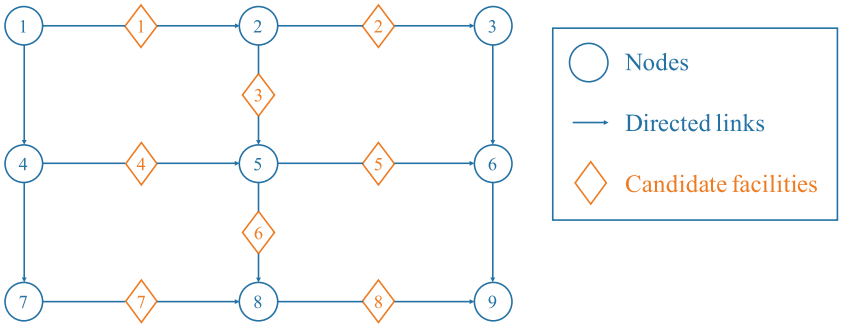

Fig. 4. The 9-node network with possible charging facilities.

solve the problem using standard NLP algorithms. In addition, we can claim that the solution of $NLP(\tau)$ as $\tau \to 0$ is a C-stationary point (Scholtes, 2001), which ensures the solution quality of our approach.

Theorem 3. *The $NLP(\tau)$ satisfies the MPEC linear independence constraint qualification (MPEC-LICQ) for any $\tau \geq 0$.*

Theorem 4 (Theorem 3.1 Scholtes, 2001)**.** *Let $\{\tau_n\}$ be a sequence of positive scalars tending to zero, let z_n be a stationary point of $NLP(\tau_n)$ tending to $\bar{z}$ and suppose MPEC-LICQ holds at $\bar{z}$, then the point $\bar{z}$ is a C-stationary point of $NLP(0)$.*

Theorem 3 follows readily from the fact that the constraints of the $NLP(\tau)$ without the complementarity constraints are linear independent. Based on Theorem 4, we present the solution algorithm, which guarantees to converge to the C-stationary point of the MPCC problem.

5. Numerical experiments

5.1. Experiment setting

In this study, numerical experiments are conducted on three test networks with various sizes and OD pairs. For all networks, we consider that the feasible routes exceed the maximal travel range L of EVs. Moreover, the travel distance from the origin to each charging facility and from each charging facility to the destination along the route are within the maximal travel range L. In this regard, all EVs have to charge at least once during each travel and are able to reach one of the charging facilities. We set charging service rate $\mu = 0.05$, which is equivalent to an average charging time of 20 min. We set waiting time $\bar{t} = 20$ and the related probability $p = 0.8$ as the service threshold, which implies that the probability that a user experiences more than 20 min of waiting is less than 80%. The unit location cost C_k^1 is set to 30, unit capacity cost C_k^2 is set to 1, and unit travel and waiting time cost C^3 is set to 2.

The first test network is a small network with 9 nodes and 12 links, as shown in Fig. 4. There are 8 candidate facility locations and 4 OD pairs, with maximum capacity for each charging facility being 20 units. The detailed network configurations can be found in Table 6. This test network is used for finalizing parameters for our solution algorithm, comparing the performance of different algorithms and evaluating solution quality.

The second test network is the Nguyen and Dupuis (1984) network with 13 nodes and 19 links, which is considered as a medium-size network for our problem. There are 19 candidate facility locations (one on each link) and 6 OD pairs, with maximum capacity for each charging facility being 20 units. The network is used for understanding the robustness of the solutions, with respect to various sets of input parameters, and providing guidance on determining facility locations when there is uncertainty in OD demand and EV market penetration rate. The detailed network configuration can be found in Tables B.10 and B.11

Finally, we introduce the Sioux-Falls network with 24 nodes and 76 links as a large-size test network. We consider 38 candidate locations and 12 OD pairs, with maximum capacity for each charging facility being 30 units. This significantly increases the scale of the problem, compared to the other two networks. We use the network to evaluate the scalability of the solution approach with various demand level, which may provide insights on how the modeling framework performs in solving real-world problems. The detailed network configuration can be found in Tables B.12 and B.13.

Algorithm 1 is implemented on the NEOS server for optimization[2], where we select IPOPT (Wächter and Biegler, 2006) as the solver for the $NLP(\tau_i)$ in the third step. The IPOPT is an interior point solver known for its excellent convergence properties and efficiency in solving large-scale NLPs (Biegler and Zavala, 2009). To illustrate the validity of our selection, we also compare the performance of IPOPT in our problem with other state-of-the-art NLP solvers, including CONOPT (Drud, 1994), FilterSQP (Fletcher and Leyffer, 2002) and Knitro (Byrd et al., 2006). Both CONOPT and FilterSQP are sequential quadratic programming (SQP) solvers, while Knitro is interior point solver. Based on our experiments, we find that CONOPT and FilterSQP always terminated at non-optimal solutions or failed to obtain a feasible solution. On the other hand, IPOPT and Knitro are consistently able to identify (local) optimal solutions with proper parameter settings. This suggests that interior point method based solvers are more suitable for solving our problems, compared to SQP based solvers. However, the solution quality of IPOPT differs from that of Knitro, which will be discussed in the next section.

Algorithm 1: Iterative algorithm for charging facility location and capacity.

Input: τ_1, τ_{stop}, start point x_0^i, and damping factor $0 < \alpha < 1$
Output: x^i, s^i

```
Set iteration number i = 1.;
while τ_i > τ_stop do
    x^i, s^i ← Solve NLP(τ_i);
    x_0^{i+1} ← x^i;
    s_0^{i+1} ← s^i;
    τ_{i+1} ← τ_i * α ;
    i ← i + 1;
end
```

[2] NEOS server for optimization: http://www.neos-server.org

Table 6
Configurations and demand profile of the 9-node network.

Link	nodes	Free-flow travel time (min)	Link capacity (veh/min)	Candidate location
1	1-4	4	3	0
2	3-6	9	4	0
3	4-7	5	4	0
4	6-9	3	2	0
5	1-2	7	3	1
6	2-3	5	4	2
7	2-5	8	5	3
8	4-5	6	3	4
9	5-6	4	2	5
10	5-8	7	3	6
11	7-8	9	5	7
12	8-9	5	4	8
OD pair	GV demand (veh/min)	EV demand (veh/min)		
1-8	1.00	0.25		
1-9	2.00	0.50		
4-9	0.80	0.20		
2-6	1.20	0.30		

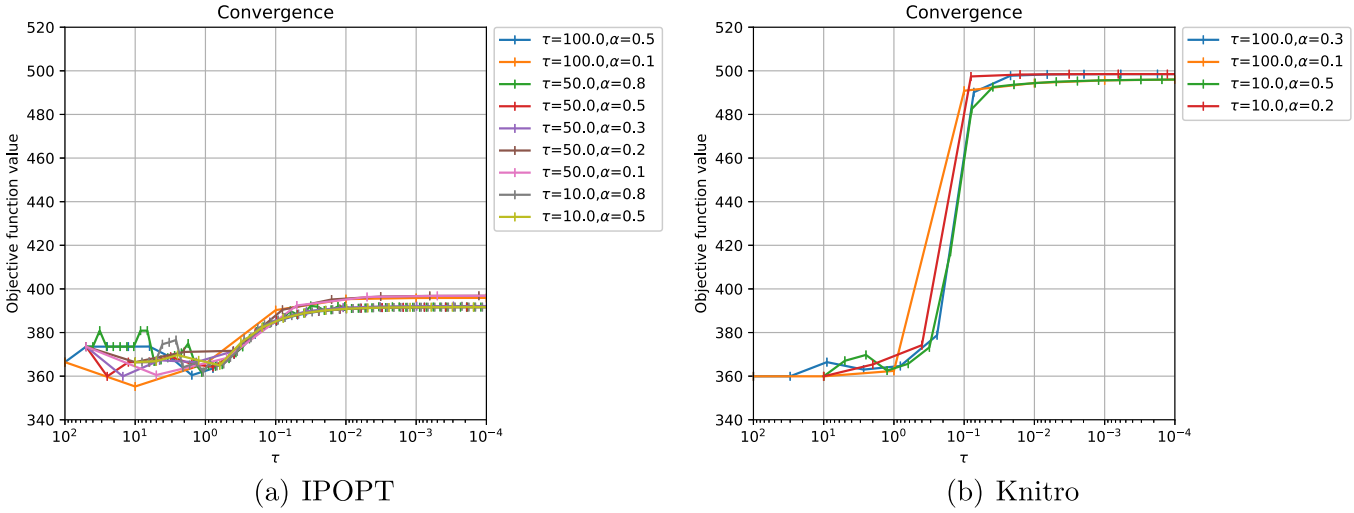

Fig. 5. Experiments on choosing relaxing components.

5.2. Solution quality

The solution quality of Algorithm 1 depends on the choice of starting value of τ, as well as the damping factor α. In general, larger values of τ and α lead to smoother relaxing of the original problem, while solutions obtained from smaller τ and α are closer to solutions of the original problem (Ban et al., 2006). We experiment with various combinations of τ and α on the small test network, and the results for both IPOPT and Knitro are shown in Fig. 5.

For IPOPT, we set τ to 10,50 and 100, and test with $\alpha = \{0.1, 0.2, 0.3, 0.5, 0.8\}$. τ_{stop} is set to $1e-5$. All parameter combinations are found to converge when the algorithm terminates, but the solutions may differ, depending on the choice of τ and α. Specifically, if we let τ be 50, and set $\alpha = 0.5$, the algorithm leads to the best solution found among all parameter settings at convergence. However, when starting τ is set to a small value, e.g., $\tau = 10$, the algorithm is found to converge to a sub-optimal solution, which is 1.32% worse than the best identified solution. Similar results are obtained for even smaller τ values. The results therefore help to identify the acceptable level of smoothness required for solving the problem, and we recommend setting τ to a larger value (e.g., $\tau = 50$) to allow sufficient smoothness for obtaining an initial solution that serves as a good warm-start point for subsequent iterations. As for Knitro, we find a similar pattern if the algorithm converges. However, Knitro may converge to infeasible solutions in 5 out of 9 trials. The four successful trials are plotted in Fig. 5(b). It can be seen that all solutions are worse than those obtained by IPOPT. These results well support our choice of IPOPT as the solver for the NLPs in our algorithm.

In addition, we compare the total computing time under different relaxing component settings, and the results are presented in Fig. 6. There are two immediate conclusions we can draw from the change of computing time. First, for the same τ value, the computing time is observed to first decrease as α increases, then starts to increase as α continues to grow larger. This is because a very small α makes the problem highly non-smooth, and the solution from the previous iteration is unlikely to be a good starting point for succeeding iterations, which increases the computational time for each iteration. In addition, it may also drive the algorithm to an inferior solution, as shown in Fig. 6(b). On the other hand, larger α values increase the smoothness of the problem, but at the cost of running significantly more iterations. Second, with a proper α value (e.g., $\alpha = 0.5$), choosing a small starting τ will also increase the time required to obtain the solution. Similar to choosing a smaller α value, a larger starting τ gives a smoother relaxation of the original problem, compared to smaller τ, and it is therefore easier to obtain the solution. However, the starting τ should not be too large either (e.g., $\tau = 100$), because it will also increase the computing time according to our previous discussion. Based on

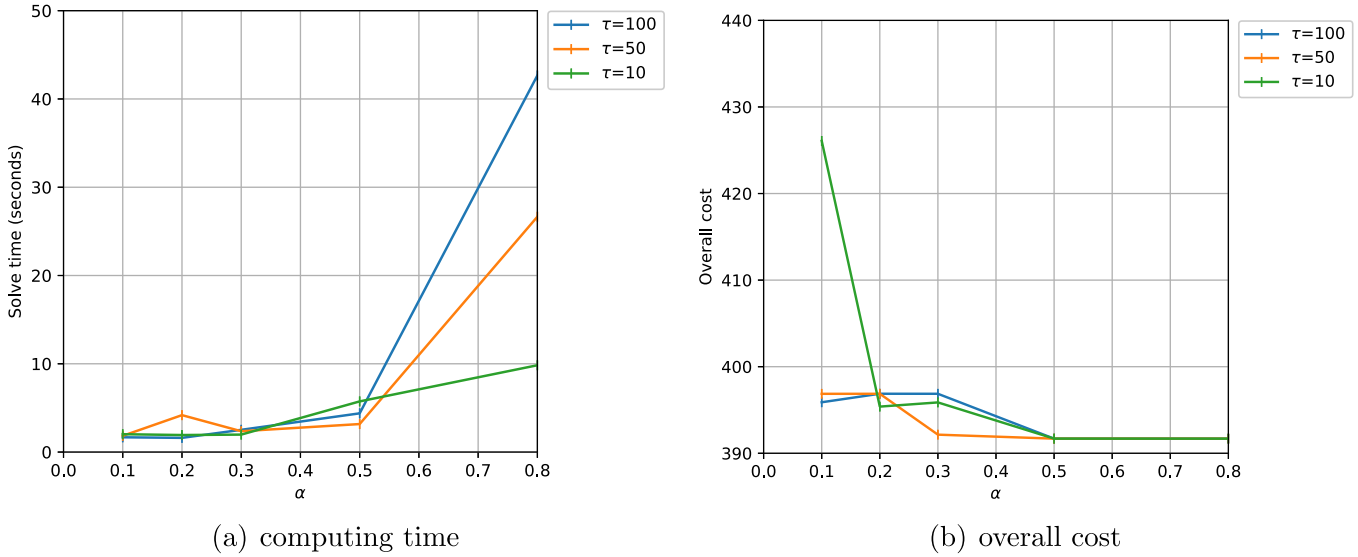

(a) computing time (b) overall cost

Fig. 6. Computing time and cost change with different settings.

Table 7
Sample results of numerical experiment. ($\tau = 50, \alpha = 0.5, \tau_{stop} = 1e-5$).

objective	391.69								
location	$x_1 = 0$	$x_2 = 1$	$x_3 = 0$	$x_4 = 0$	$x_5 = 0$	$x_6 = 1$	$x_7 = 1$	$x_8 = 0$	
capacity	$s_1 = 0$	$s_2 = 15.159$	$s_3 = 0$	$s_4 = 0$	$s_5 = 0$	$s_6 = 17.042$	$s_7 = 17.042$	$s_8 = 0$	
allocation	facility1	facility2:	facility3:	facility4:	facility5:	facility6:	facility7:	facility8:	
EV flow	0	0.368	0	0	0	0.441	0.441	0	
GOD	Route	Travel	Flow	EOD	Route	Travel	Waiting	Total	Flow
1-8	1-2-5-8	22.00	0	1-	1-2-5-8	22.00	2.86	24.86	0
	1-4-5-8	19.39	1.000	8	1-4-5-8	19.39	2.86	22.25	0.250
	1-4-7-8	19.39			1-4-7-8	19.39	2.86	22.25	
1-9	1-2-5-8-9	27.00	0	1-	1-2-5-8-9	27.00	2.86	29.86	0
	1-2-5-6-9	26.21	0	9					
	1-4-5-6-9	23.60	2.000						
	1-2-3-6-9	25.95	0		1-2-3-6-9	25.95	1.30	27.25	0.500
	1-4-5-8-9	24.39	0		1-4-5-8-9	24.39	2.86	27.25	
	1-4-7-8-9	24.39	0		1-4-7-8-9	24.39	2.86	27.25	
4-9	4-5-6-9	18.24	0.800	4-					
	4-5-8-9	19.03	0	9	4-5-8-9	19.03	2.86	21.89	0.200
	4-7-8-9	19.03	0		4-7-8-9	19.03	2.86	21.89	
2-6	2-3-6	14.05	1.200	2-	2-3-6	14.05	1.30	15.35	0.300
	2-5-6	14.31	0	6					

* GOD: OD pair of GV. EOD: OD pair of EV. Flow: (veh/min).
Travel: travel time (min). Waiting: waiting time (min). Total: total time (min).

these results, we select $\tau = 50$ and $\alpha = 0.5$ as the optimal parameter setting for our problem. This parameter setting is used for the following experiments in this study.

Based on the results of relaxing components and computing time, we set initial $\tau = 50$ and $\alpha = 0.5$, and present the converging solution, as shown in Table 7. The algorithm converges after 23 iterations, which takes 3.17 CPU seconds. The results suggest that constructing 3 facilities (candidate location 2,6,7) gives the (local) optimal solution, with capacity for each facilities being 15.159, 17.042 and 17.042 respectively. The result very well satisfies the integer constraints.

Moreover, the flow is observed to be distributed over routes and charging facilities of the lowest cost for each OD pair, with higher cost options being unvisited. The formulation of our CRC Equilibrium is thus verified to be correct. These also imply that the algorithm is capable of identifying solutions effectively, with the solutions being feasible and satisfying all regular and complementarity constraints (as shown in Fig. 7).

We further evaluate the solution quality as compared to the solutions obtained from enumerations in Table 8. In this experiment, we compare the solutions obtained from Algorithm 1 by solving the original $NLP(\tau)$ versus the solutions obtained from Algorithm 1 on solving $NLP(\tau)$ with given facility locations. That is, we enumerate all possible facility location strategies and make it as an input, then solve the $NLP(\tau)$ by optimizing only the capacity at each facility. This significantly reduces the complexity of the original problem, and we use the best solution obtained from location enumeration as the benchmark solution. The pseudo-code for implementing Algorithm 1 on location enumeration is presented in Algorithm 2 , and we have enumerated all 2^8 possible combinations for each scenario on the small test network.

To comprehensively understand the performances, we create 9 scenarios by varying C^3 and η level, and the results are shown in Table 8. It can be observed that, the highest difference is reported to be 1.64%, with the average difference over the 9 scenarios being 0.62%, and it saves hundredfold computing time. These demonstrate the effectiveness and efficiency of Algorithm 1 in obtaining optimal or near-optimal solutions and show that the algorithm is able to generate reliable facility location plans when it is impossible to enumerate all possible combinations in real-world cases.

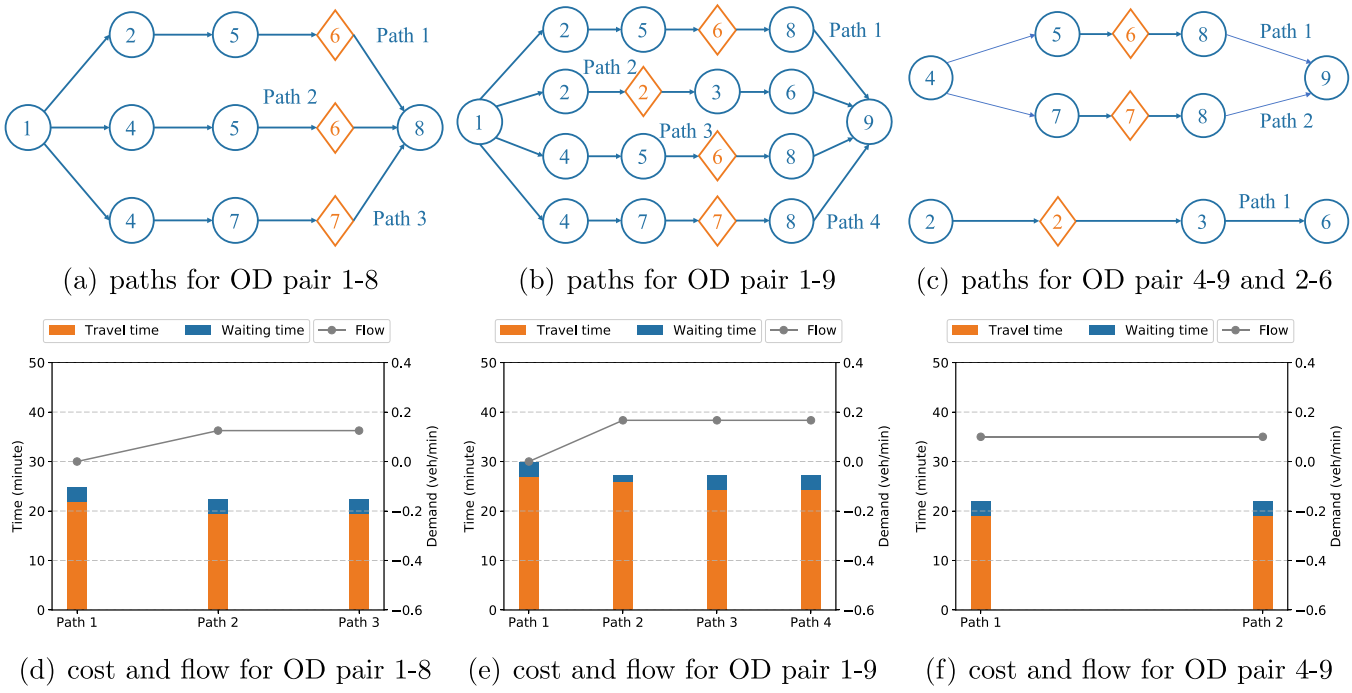

(a) paths for OD pair 1-8 (b) paths for OD pair 1-9 (c) paths for OD pair 4-9 and 2-6

(d) cost and flow for OD pair 1-8 (e) cost and flow for OD pair 1-9 (f) cost and flow for OD pair 4-9

Fig. 7. Cost and flow of paths for each OD pair.

Table 8
Comparison of the results and best solutions. ($\tau = 50, \alpha = 0.5, \tau_{stop} = 1e-5$).

	(C^3, G: E)	(1, 1: 1)	(2, 1: 1)	(3, 1: 1)	(1, 2: 1)	(2, 2: 1)
overall cost	Algorithm 1	350.23	452.14	555.23	207.01	278.81
	best solution	350.23	452.14	553.21	205.77	274.31
	gap	0.00%	0.00%	0.37%	0.61%	1.64%
solve time (s)	Algorithm 1	5.06	4.04	2.77	5.10	4.88
	best solution	474.64	667.79	311.66	343.20	390.73
	proportion	1:94	1:165	1:113	1:67	1:80
	(C^3, G: E)	(3, 2: 1)	(1, 4: 1)	(2, 4: 1)	(3, 4: 1)	average
overall cost	Algorithm 1	346.37	264.48	391.68	523.24	-
	best solution	344.72	264.48	391.68	517.43	-
	gap	0.48%	0.00%	0.00%	1.11%	0.62%
solve time (s)	Algorithm 1	4.83	2.91	3.17	4.40	-
	best solution	465.12	347.62	390.19	394.46	-
	proportion	1:96	1:119	1:123	1:90	1:105

* G: GV demand. E: EV demand.

5.3. Sensitivity analysis

In this subsection, we discuss the robustness of the solutions from the following three aspects: (a) the impact on the choice of C^3, (b) the impact of different demand level D and (c) the impact of different EV penetration rate. We focus on these factors since they are usually associated with the highest uncertainty in real-world problems. On one hand, agencies may have different perceptions over the value of construction cost and travel cost. These values may have significant impact on the property of the objective function since the construction cost takes linear form while the charging time is an exponential function of EV demand. On the other hand, the demand level and EV penetration rate may change over time, and we may expect the implemented location and capacity strategy to be well-suited for a range of demand and penetration level. These two values are closely associated with the equilibrium solution in the lower-level of the original problem.

We evaluate the impact of C^3 on solution quality using the small test network, and the results are presented in Fig. 8. In Fig. 8, we fix the value of $C^1 = 30$ and only vary the value of C^3. The overall trend is that we tend to invest more on facilities with higher value of charging and travel time, and the construction cost follows the law of diminishing marginal utility. Time cost can barely be reduced by increasing construction investment when C^3 reaches some level (e.g., $C^3 = 2$), because all feasible candidate locations are constructed with full capacity when C^3 exceeds the threshold.The results indicate that the model is robust to a wide range of C^3 values, unless certain extreme values are taken for C^3.

We next conduct experiments to understand how input flow D may affect the solutions on the medium-size network (the NguyenDupuis network). We test with D varying between 4.10 and 20.50, with all other parameters unchanged. The changes of objective function value and number of facilities are shown in Fig. 9. It can be seen in Fig. 9(a) that the overall cost increases monotonically as the demand level increases, however, the number of facilities resembles the piece-wise-linear shape with respect to higher demand. This implies that the location plan is robust to a wide range of flow values (e.g., same number of facilities for demand between [4.10,5.74],[7.38,10.66],[12.30,13.94],[15.58,20.50]), and we only need to vary the capacity at each location to satisfy the travel needs of higher demand, which is reflected by the construction cost curve in Fig. 9(b). While adjusting capacity at facilities is much

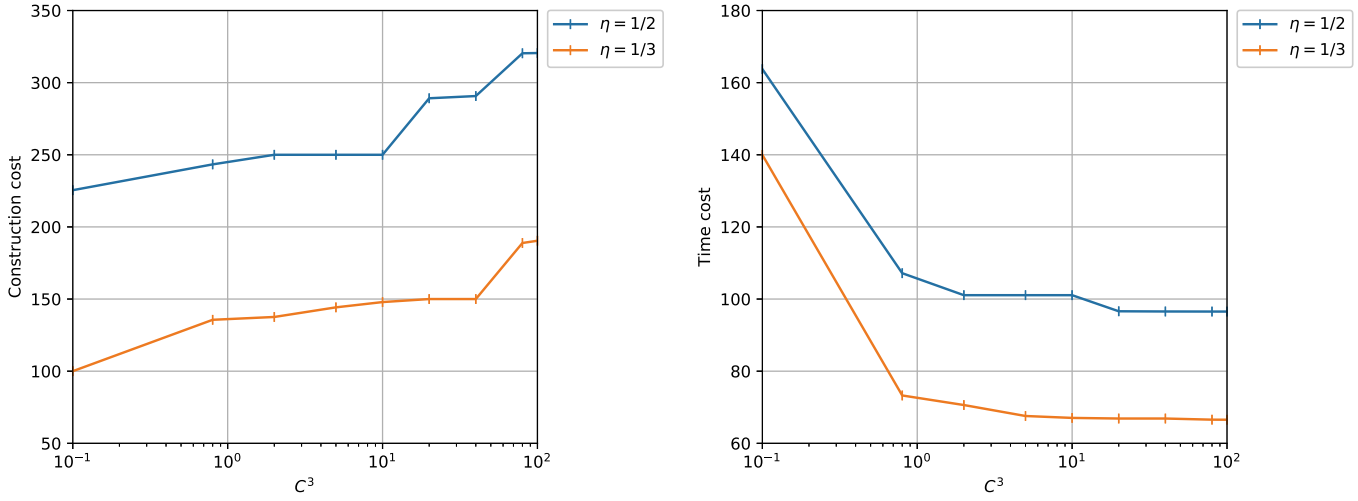

(a) construction cost (b) time cost

Fig. 8. cost changes with increasing C^3 (9 nodes, $\tau = 50, \alpha = 0.5, \tau_{stop} = 1e-5$).

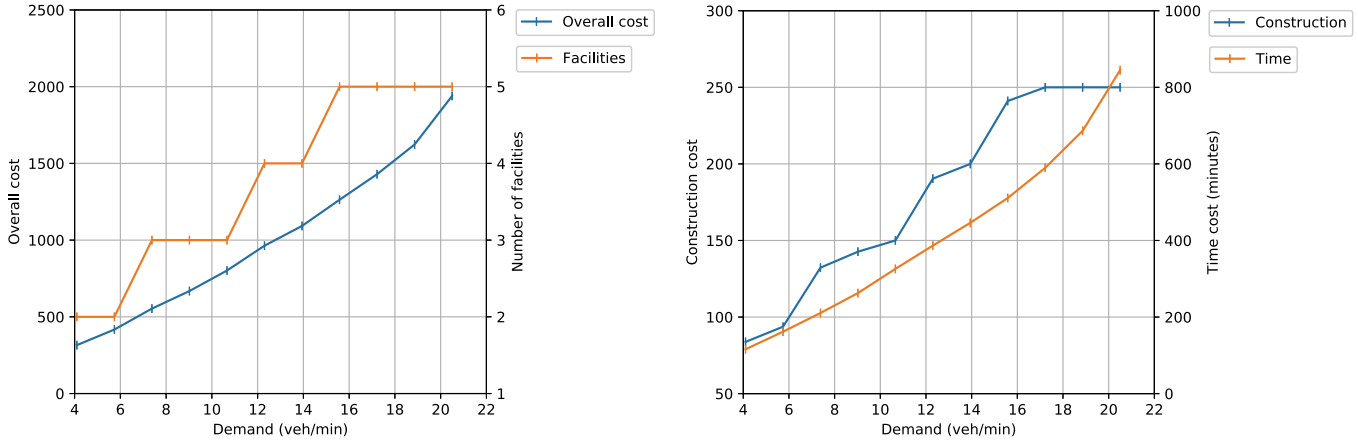

(a) overall cost and facilities (b) construction and time cost

Fig. 9. Cost changes with different OD demand (13 nodes, $\tau = 100, \alpha = 0.5, \tau_{stop} = 1e-4$).

Algorithm 2: Capacity optimization with location enumeration.

Input: Candidate location set X, powerset of candidate location set $P(X)$, facilities location set X^*, τ_1, τ_{stop}, start point x_0^i, and damping factor $0 < \alpha < 1$

Output: x^*, s^*

```
for X* ∈ P(X) do
    Set iteration number i = 1, set Obj* as an arbitrary large number;
    while τ_i > τ_stop do
        x^i, s^i, Obj ← Solve NLP(τ_i, x_0^i, s_0^i);
        x_0^{i+1} ← x^i;
        s_0^{i+1} ← s^i;
        τ_{i+1} ← τ_i * α ;
        i ← i + 1;
    end
    if Obj < Obj* then
        x* = x^i, s* = s^i;
    end
end
```

more cost-effective than changing facility locations, we may conclude that the location and capacity design derived from our model is also robust to the change of demand level. With the derived construction plan, we also observe a near-perfect linear relationship between OD demand and total time cost, which suggests that each individual may experience the same level of service with the increase in total demand level.

EV market penetration rate η is another important parameter which affects the time cost, even under the same demand level, and we present the sensitivity analysis of solution quality with respect to η in Fig. 10. In this experiment, we are also interested in the change of waiting time as it measures the level of service for EVs. It can be observed from Fig. 10(b) that the overall cost increases with higher penetration rate under the same demand level and the travel time cost stays stable while the waiting time cost increases with increasing η. Note that the waiting time increases exponentially with increasing EV demand, and the impact of the change in waiting time cost is more significant on the change in EV flow at each facility when the penetration rate is high (e.g., $\eta = 60\%$). In terms of solution robustness, we observe that the number of locations may be stable for a small interval of EV market penetration rates (e.g., 9 facilities for $\eta \in [0.404, 0.444]$,

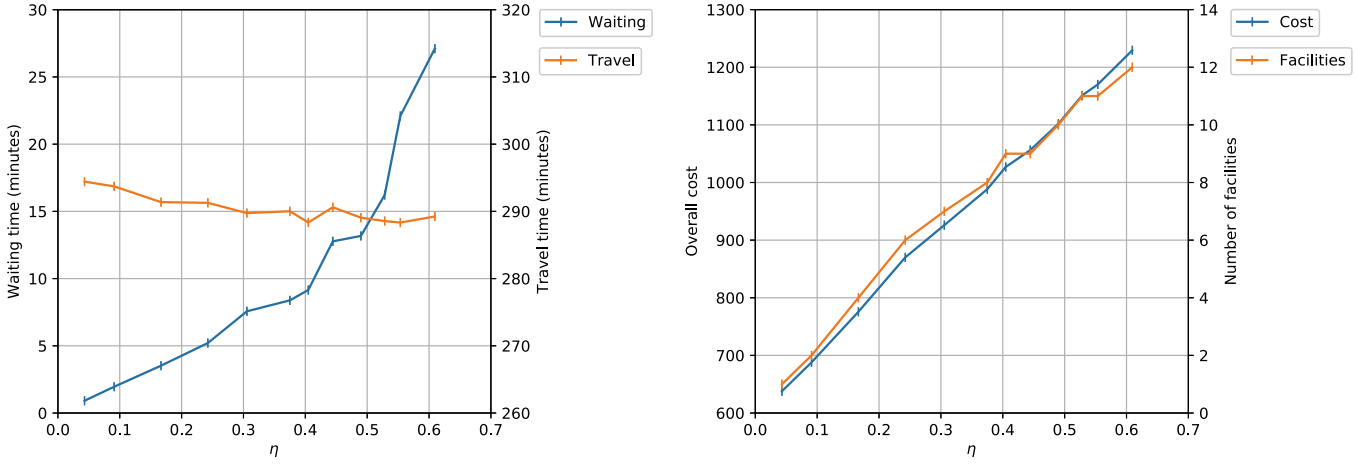

(a) waiting and travel time cost (b) overall cost and number of facilities

Fig. 10. Cost changes with different level of η (13 nodes, $\tau = 100, \alpha = 0.5, \tau_{stop} = 1e-4$).

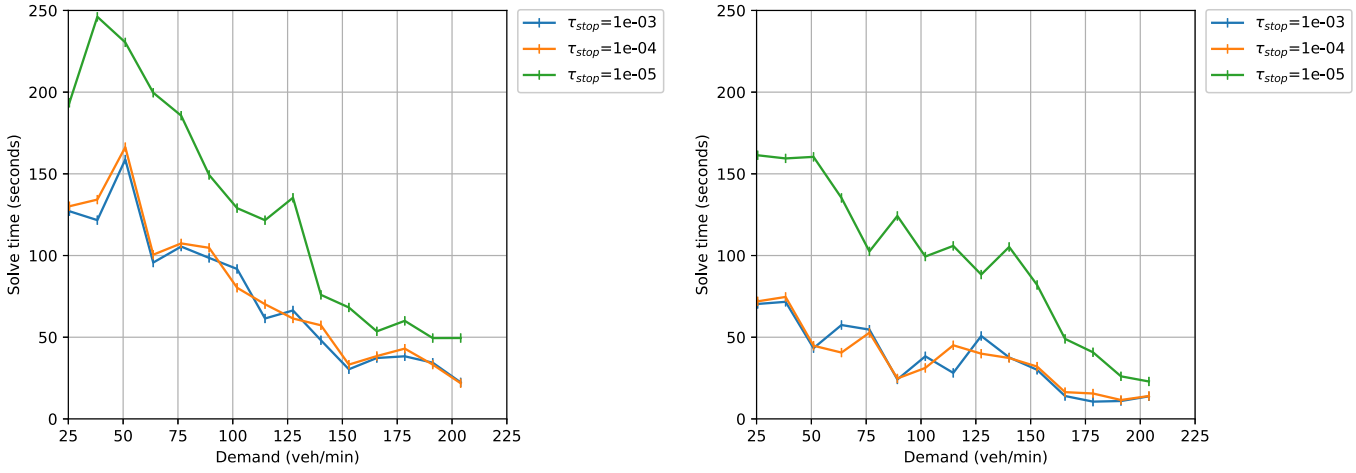

(a) $\eta = 1/(1+50)$ (b) $\eta = 1/(1+30)$

Fig. 11. Total computing time changes with different OD demand (24 nodes, $\tau = 10^3, \alpha = 0.5$).

11 facilities for $\eta \in [0.528, 0.553]$). While the EV market penetration may grow exponentially faster with technology advances and the stimulating of policies, we conclude that it will be more effective to allow for a large buffer in terms of EV market penetration rate in determining optimal charging facility plans.

5.4. Performance on large network

We next evaluate the total computing time under different OD demand on the Sioux-Falls network. The changes of total computing time are shown in Fig. 11. For the parameter settings of the large network, we observe that using the same τ ($\tau = 50$ or $\tau = 100$) may lead to convergence towards inferior solutions or even infeasible points, which is likely due to the lack of smoothness with increased problem size. As a consequence, we set $\tau = 10^3$ for the experiments. We compare three stopping criteria ($\tau_{stop} = 1e-3$, $\tau_{stop} = 1e-4$, and $\tau_{stop} = 1e-5$) to understand how the computing time and solution quality may change. Based on the results, we find that all τ_{stop} values give the same solutions (difference between objective function values being smaller than $1e-6$). However, $\tau_{stop} = 1e-3$ and $\tau_{stop} = 1e-4$ require similar computing time, while the smaller τ_{stop} value (i.e., $\tau_{stop} = 1e-5$) may require twice as much computing time. As a result, $\tau_{stop} = 1e-4$ is sufficient to obtain accurate solutions for the large network.

We observe that total computing time does not strictly increase with the growth of driver demand. Instead, the change of computing time has two phases. When EV demand $D_e = \eta \cdot D < 1$, the computing time may increase with growing demand. When EV demand $D_e > 1$, the computing time may decrease significantly. The reason is two-fold. First, when charging demand is at a low level, the computing time it takes is primarily for searching in the wide feasible region, which makes the computing time increase with growing demand. Second, when the network is not congested, the feasible solution space is much wider than when it is congested, which makes it more difficult to find the equilibrium flow.

Therefore, we claim that the scalability is at an acceptable level since the total computing time does not increase significantly when OD demand increases and it only doubles when the accuracy parameter τ_{stop} changes from $1e-3$ to $1e-5$. As for the comparison of computing time across different networks, we find that the computing time increases exponentially with the size of the network (e.g., 3.17s on small network with $D_e = 1.25$, 5.31s on medium network with $D_e = 1.5$ and 81.98s with $D_e = 5$ on large network). However, even for the largest network with the highest

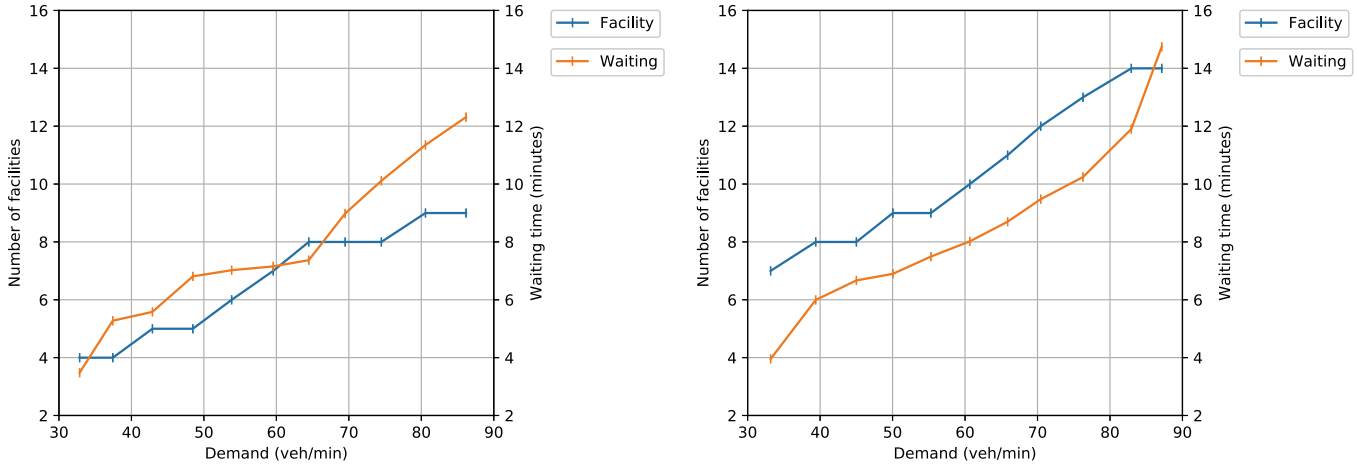

(a) $\eta = 1/(1+15)$ (b) $\eta = 1/(1+10)$

Fig. 12. Waiting time changes with different OD demand (24 nodes, $\tau = 10^3, \alpha = 0.5, \tau_{stop} = 1e-3$).

demand in our numerical experiments, the total computing time is about 246 seconds, which implies that our model is practicable for real-world networks.

We also conduct experiments to see how the input flow D affects the solution and the average waiting time on the large network. We tested with D varying between 32.85 and 86.17, with all other parameters unchanged ($\tau = 10^3, \alpha = 0.5, \tau_{stop} = 1e-3$). The changes of average waiting time and number of facilities are shown in Fig. 12. The average waiting time for all the demand levels is less than 15 min (3.48 mins minimum, 14.74 maximum), and it increases as the demand increases with the fixed number of facilities. The shape of the facility amount curve just reaches the same conclusion we draw on the medium-size network.

Finally, we notice that heuristic algorithm (e.g., Fernandes et al., 2014 and Tran et al., 2018) is also a popular alternative for location problems on large-scale networks and the algorithms can find acceptable solutions for the integer programs in relatively short time. However, the lower-level problems in most of the heuristic approaches are usually much simpler (normally linear programs) than that of ours (network flow equilibrium problem), which is cheap to evaluate and therefore suits well into the heuristic framework. To compare the effectiveness and efficiency of our algorithm (Algorithm 1) with heuristic approaches, a local-search based heuristic (as shown in Algorithm 3) is implemented on the same instances, which is reported to produce high-quality solutions for a large collection of optimal facility location problems (Halper et al., 2015). For the local-search heuristic, we define a basic neighborhood involving three types (Chang et al., 2007): (1) opening one new facility, (2) closing one opened facility, and (3) opening one new facility while closing an opened one. In order to better assess the quality of the solutions for large networks, we also evaluate the lower bound of our problem by relaxing the binary constraints from location decision variables in the upper-level and define the gap between the solutions obtained from the algorithms and the lower bound as:

$$Gap = \frac{Optimal - LowerBound}{LowerBound} \times 100\% \tag{37}$$

Both algorithms and the problem with relaxed integer constraints have been evaluated over various demand levels (between 2.8 and 45.9) on all three networks to compare their performances. We set $\tau = 50, \alpha = 0.5, \tau_{stop} = 1e-5$ on the small network (9 nodes), $\tau = 100, \alpha = 0.5, \tau_{stop} = 1e-4$ on the NguyenDupuis network (13 nodes) and $\tau = 10^3, \alpha = 0.5, \tau_{stop} = 1e-3$ on the Sioux-Falls network (24 nodes). The results are shown in Table 9, from

Algorithm 3: Local-search based heuristic.

Input: set of neighbors N, initial solution $\hat{x}_0$, and damping factor $0 < \alpha < 1$
Output: x^*, s^*
Set $\hat{x} = \hat{x}_0$;**while** *the stopping criterion is not true* **do**
  for $x \in N(\hat{x})$ **do**
    Set iteration number $i = 1$, set Obj^* as an arbitrary large number;
    while $\tau_i > \tau_{stop}$ **do**
      $x^i, s^i, Obj \leftarrow$ Solve $NLP(\tau_i, x, s_0^i)$;
      $x_0^{i+1} \leftarrow x^i$;
      $s_0^{i+1} \leftarrow s^i$;
      $\tau_{i+1} \leftarrow \tau_i * \alpha$;
      $i \leftarrow i + 1$;
    end
    if $Obj < Obj^*$ **then**
      $x^* = x^i, s^* = s^i$;
    else
      if *it passes the acceptance test* **then**
        $x^* = x^i, s^* = s^i$;
      end
    end
  end
  Let $\hat{x} = x^*$;
end

which we can draw the following conclusion. First, compared to Algorithm 3, Algorithm 1 is able to obtain better solutions with less cost in shorter time under the same circumstances and the solution quality is acceptable with the average gap 6.83%. Second, when the network size increases, the heuristic algorithm fails to obtain acceptable solutions in a timely manner as evaluating the lower-level problem becomes much more expensive. On the other hand, the relaxed NLP which provides the solution lower bound can still be solved effectively and are observed to be not far from the solution generated by our algorithm.

6. Conclusions

In this study, we formulated the optimal location and capacity design of EV charging facilities as a bi-level programming problem. The model explicitly considers the waiting time at each charging

Table 9
Comparison of the results from different algorithms.

		Algorithm 1	Gap	Algorithm 3	Gap	Lower bound	
9 nodes	D = objective	183.28	4.96%	183.38	5.01%	174.62	
	2.8 solve time (s)	5.82	-	12.19	-	0.04	
	D = objective	224.28	6.94%	224.64	7.11%	209.73	
	3.8 solve time (s)	3.61	-	10.58	-	0.05	
	D = objective	244.54	5.65%	244.93	5.82%	231.47	
	4.3 solve time (s)	7.86	-	17.21	-	0.05	
13 nodes	D = objective	454.13	5.31%	454.68	5.44%	431.22	
	4.8 solve time (s)	11.31	-	74.17	-	0.06	
	D = objective	536.40	4.45%	548.56	6.81%	513.56	
	6.3 solve time (s)	8.99	-	70.07	-	0.03	
	D = objective	619.96	3.58%	621.92	3.91%	598.51	
	7.8 solve time (s)	7.41	-	51.61	-	0.07	
24 nodes	D = objective	1467.97	18.38%	1646.05	32.74%	1240.05	
	27.5 solve time (s)	55.74	-	667.85	-	2.03	
	D = objective	1762.76	6.87%	2189.14	32.71%	1649.51	
	36.7 solve time (s)	72.49	-	580.11	-	2.92	
	D = objective	2236.65	5.34%	2730.03	28.58%	2123.21	
	45.9 solve time (s)	69.88	-	740.79	-	3.13	

facility and the greedy behavior of EV drivers in route and charging facility choices. We proposed approximation methods to model the waiting probability and average waiting time of the $M(t)/M/n$ queue, reformulated the problem as a single-level NLP and developed the component relaxing algorithm to solve the NLP iteratively.

Numerical experiments were conducted on three networks with different sizes for choosing relaxing components, evaluating solution quality, analyzing sensitivity of parameters and assessing robustness of solutions. In particular, our algorithm is found to be efficient in obtaining effective solutions if relaxing components are chosen properly. In addition, the solutions are observed to be robust to various demand level and different cost perceptions of travel and waiting time. Finally, the proposed model and solution algorithm may be implemented for solving real-world problems with good scalability on large networks.

The study also has several limitations, which we plan to improve in our future work. First, while mixed environment of EVs and gas vehicles is modeled, all EVs are considered homogeneous. We will investigate the market of different EV products with various travel range to understand how the charging and routing equilibrium may differ. Second, while the current solution algorithm is found to be effective and efficient, we also identified the existence of gaps between the current solutions and the best enumerated ones. Future efforts can be made to improve the algorithm performance, with special attention to the exponential structure of the average waiting time functionn. In addition, other NLP reformulations of the MPCC in our study can be exercised to compare the solution quality and computing efficiency. Finally, we would like to combine our theoretical model with survey data and conduct experiments in real-world networks to help draft practical plans for charging facility locations.

Acknowledgement

The first authors work is supported by the China Scholarship Council during his stay at Purdue University and the National Natural Science Foundation of China (no. 71771130). The authors are grateful for the support. The findings are the responsibility of the authors alone.

Appendix A. Proof

Proof of Proposition 1.

Proof. It is easy to verify that Eq. (22) holds according to Eq. (20). In the following we present the proof for Eq. (21). Let $y(x) = \alpha_k{}^x e^{-\alpha_k} - \alpha_k'{}^x e^{-\alpha_k'}$ for $x \geq 0$, where $0 < \alpha_k < \alpha_k'$ ($s_k < s_k'$). As $y(x) = \alpha_k{}^x e^{-\alpha_k}(1 - \left(\frac{\alpha_k'}{\alpha_k}\right)^x e^{\alpha_k - \alpha_k'})$, $0 < \alpha_k < \alpha_k'$, there exists $x^* > 0$ such that $\begin{cases} y(x) \geq 0 & 0 \leq x \leq x^* \\ y(x) \leq 0 & x \geq x^* \end{cases}$. Thus, there exists an integer j^* such that:

$$\begin{cases} \frac{\alpha_k{}^j e^{-\alpha_k}}{j!} \geq \frac{\alpha_k'{}^j e^{-\alpha_k'}}{j!} & 0 \leq j \leq j^* \\ \frac{\alpha_k{}^j e^{-\alpha_k}}{j!} \leq \frac{\alpha_k'{}^j e^{-\alpha_k'}}{j!} & j \geq j^* + 1 \end{cases}$$

As $\sum_{j=0}^{\infty} \frac{\alpha_k{}^j e^{-\alpha_k}}{j!} = \sum_{j=0}^{\infty} \frac{\alpha_k'{}^j e^{-\alpha_k'}}{j!} = 1$, $\sum_{j=0}^{j^*} \left(\frac{\alpha_k{}^j e^{-\alpha_k}}{j!} - \frac{\alpha_k'{}^j e^{-\alpha_k'}}{j!}\right) = \sum_{j=j^*+1}^{\infty} \left(\frac{\alpha_k'{}^j e^{-\alpha_k'}}{j!} - \frac{\alpha_k{}^j e^{-\alpha_k}}{j!}\right) \geq 0$. Then:

$$\begin{aligned}
&G_k(s_k, \lambda_k) - G_k(s_k', \lambda_k) \\
&= \sum_{j=0}^{j^*} P_{k,j} \left(\frac{\alpha_k{}^j e^{-\alpha_k}}{j!} - \frac{\alpha_k'{}^j e^{-\alpha_k'}}{j!}\right) \\
&\quad + \sum_{j=j^*+1}^{\infty} P_{k,j} \left(\frac{\alpha_k{}^j e^{-\alpha_k}}{j!} - \frac{\alpha_k'{}^j e^{-\alpha_k'}}{j!}\right) \\
&\geq P_{k,j^*} \sum_{j=0}^{j^*} \left(\frac{\alpha_k{}^j e^{-\alpha_k}}{j!} - \frac{\alpha_k'{}^j e^{-\alpha_k'}}{j!}\right) \\
&\quad + \sum_{j=j^*+1}^{\infty} P_{k,j} \left(\frac{\alpha_k{}^j e^{-\alpha_k}}{j!} - \frac{\alpha_k'{}^j e^{-\alpha_k'}}{j!}\right) \\
&= P_{k,j^*} \sum_{j=j^*+1}^{\infty} \left(\frac{\alpha_k'{}^j e^{-\alpha_k'}}{j!} - \frac{\alpha_k{}^j e^{-\alpha_k}}{j!}\right) \\
&\quad + \sum_{j=j^*+1}^{\infty} P_{k,j} \left(\frac{\alpha_k{}^j e^{-\alpha_k}}{j!} - \frac{\alpha_k'{}^j e^{-\alpha_k'}}{j!}\right) \\
&\geq \sum_{j=j^*+1}^{\infty} P_{k,j} \left(\frac{\alpha_k'{}^j e^{-\alpha_k'}}{j!} - \frac{\alpha_k{}^j e^{-\alpha_k}}{j!}\right) \\
&\quad + \sum_{j=j^*+1}^{\infty} P_{k,j} \left(\frac{\alpha_k{}^j e^{-\alpha_k}}{j!} - \frac{\alpha_k'{}^j e^{-\alpha_k'}}{j!}\right) = 0
\end{aligned}$$

Since $s_k < s_k'$, this suggests that $G_k(s_k, \lambda_k)$ is non-decreasing with respect to s_k. This completes the proof. □

Proof of Proposition 2.

Proof. We first show that the $SOL(CP(\mathcal{H}(x,s),F))$ is nonempty-valued, compact-valued and upper semi-continuous point-to-set map. It is obvious that the link travel time cost function is strictly monotone and the average waiting time function $\bar{W}_k^2(\lambda_{e,k}, s_k)$ is strictly monotone, considering s_k is fixed. Therefore, $F(\lambda, x, s)$ is a parameterized-strictly-monotone function with x and s being the given parameters. Since the waiting time probability function is in linear form, all constraints are parameterized-linear and linearly independent from each other, we conclude that $CP(\mathcal{H}(\bar{x},\bar{s}),F)$ has a unique solution with any given $\bar{x},\bar{s}$. Therefore, $SOL(CP(\mathcal{H}(\bar{x},\bar{s}),F))$ is compact and nonempty, given $\bar{x}$ and $\bar{s}$, and the point-to-set map $SOL(CP(\mathcal{H}(x,s),F))$ is nonempty-valued, compact-valued and continuous point-to-set map.

Second, since the constraints (28) and (29) are all linear, the Cartesian product of compact sets are still compact. Moreover, the objective function (27) of the MPCC is continuous. Following Corollary 1 in Harker and Pang (1988), we arrive at the conclusion that the MPEC (27) and (30) has at least one optimal solution if the feasible set is non-empty. □

Appendix B. Configurations of the networks

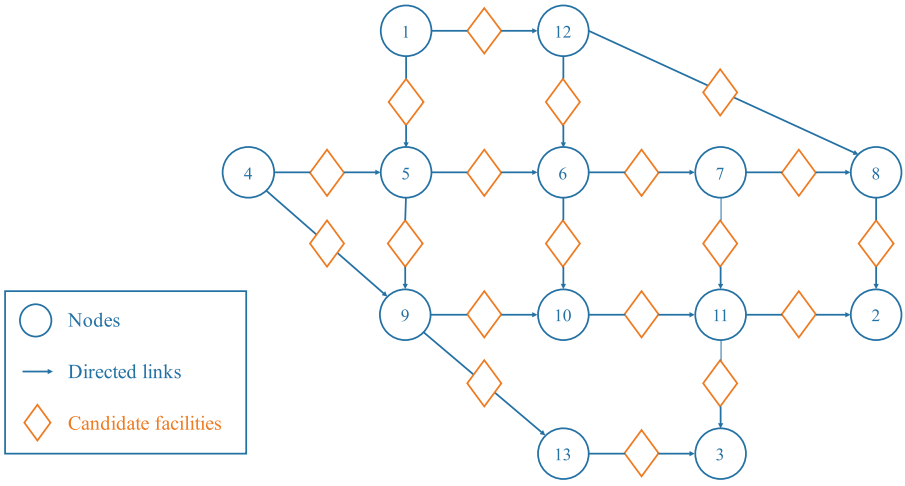

Fig. B.13. The NguyenDupuis network with possible charging facilities.

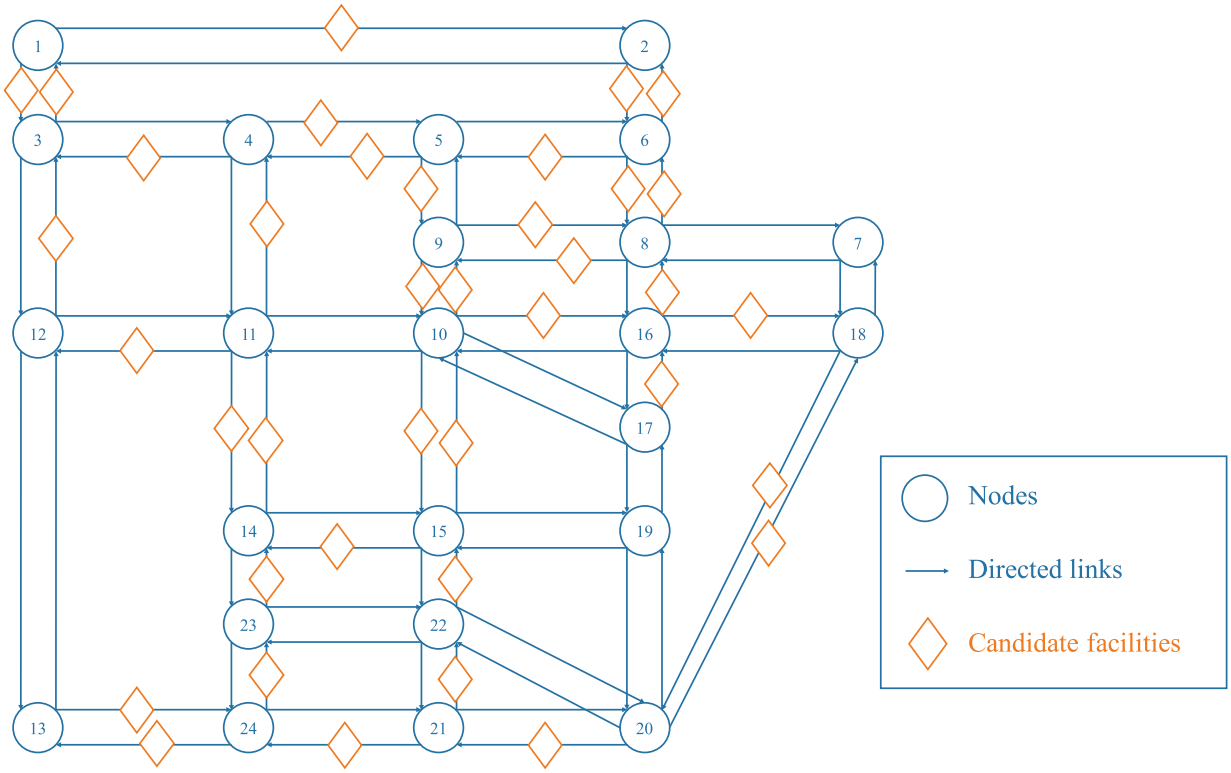

Fig. B.14. The Sioux-Falls network with possible charging facilities.

Table B.10
Configurations of the NguyenDupuis network.

Link:nodes	FTT	LC	CL	Link:nodes	FTT	LC	CL	Link:nodes	FTT	LC	CL
1: 1-5	7	300	1	8: 6-10	13	250	1	14: 10-11	6	400	1
2: 1-12	9	200	1	9: 7-8	5	250	1	15: 11-2	9	300	1
3: 4-5	9	200	1	10: 7-11	9	300	1	16: 11-3	8	300	1
4: 4-9	12	200	1	11: 8-2	9	500	1	17: 12-6	7	200	1
5: 5-6	3	350	1	12: 9-10	10	550	1	18: 12-8	14	300	1
6: 5-9	9	400	1	13: 9-13	9	200	1	19: 13-3	11	200	1
7: 6-7	5	500	1								

* Free-flow Travel Time (FTT, min), Link Capacity (LC, veh/h), Candidate Location (CL).

Table B.11
Demand profile of the NguyenDupuis network.

OD pair	GV Demand	EV Demand	OD pair	GV Demand	EV Demand
1: 1-2	90	6	4: 4-3	90	27
2: 1-3	60	6	5: 5-11	90	27
3: 4-2	120	12	6: 12-11	30	12

* Demand (veh/h)

Table B.12
Demand profile of the Sioux-Falls network.

OD pair	GV Demand	EV Demand	OD pair	GV Demand	EV Demand
1: 1-18	12.92	12.92η	7: 13-18	11.46	11.46η
2: 2-15	12.71	12.17η	8: 14-6	13.20	13.20η
3: 4-20	12.18	12.18η	9: 15-2	14.11	14.11η
4: 5-13	12.51	12.51η	10: 19-4	13.31	13.31η
5: 10-23	13.51	13.51η	11: 20-3	11.70	0
6: 11-2	13.41	13.41η	12: 21-11	11.93	0

* Demand (10^2veh/h)

Table B.13
Configurations of the Sioux-Falls network.

Link:nodes	FTT	LC	CL	Link:nodes	FTT	LC	CL	Link:nodes	FTT	LC	CL
1: 1-2	1.8	6.02	1	27: 10-11	1.5	20	0	52: 17-16	0.6	10.46	1
2: 1-3	1.2	9.01	1	28: 10-15	1.8	27.02	1	53: 17-19	0.6	9.65	0
3: 2-1	1.8	12.02	0	29: 10-16	1.5	10.27	1	54: 18-7	0.6	46.81	0
4: 2-6	1.5	15.92	1	30: 10-17	2.1	9.99	0	55: 18-16	0.9	39.36	0
5: 3-1	1.2	46.81	1	31: 11-4	1.8	9.82	1	56: 18-20	1.2	8.11	1
6: 3-4	1.2	34.22	0	32: 11-10	1.5	20	0	57: 19-15	1.2	4.42	0
7: 3-12	1.2	46.81	0	33: 11-12	1.8	9.82	1	58: 19-17	0.6	9.65	0
8: 4-3	1.2	25.82	1	34: 11-14	1.2	9.75	1	59: 19-20	1.2	10.01	0
9: 4-5	0.6	28.25	1	35: 12-3	1.2	46.81	1	60: 20-18	1.2	8.11	1
10: 4-11	1.8	9.04	0	36: 12-11	1.8	9.82	0	61: 20-19	1.2	6.05	0
11: 5-4	0.6	46.85	1	37: 12-13	0.9	51.80	0	62: 20-21	1.8	10.12	1
12: 5-6	1.2	13.86	0	38: 13-12	0.9	51.80	0	63: 20-22	1.5	10.15	0
13: 5-9	1.5	10.52	1	39: 13-24	1.2	10.18	1	64: 21-20	1.8	10.12	0
14: 6-2	1.5	9.92	1	40: 14-11	1.2	9.75	1	65: 21-22	0.6	10.46	1
15: 6-5	1.2	9.90	1	41: 14-15	1.5	10.26	0	66: 21-24	0.9	9.77	1
16: 6-8	0.6	21.62	1	42: 14-23	1.2	9.85	0	67: 22-15	1.2	20.63	1
17: 7-8	0.9	15.68	0	43: 15-10	1.8	27.02	1	68: 22-20	1.5	10.15	0
18: 7-18	0.6	46.81	0	44: 15-14	1.5	10.26	1	69: 22-21	0.6	10.46	0
19: 8-6	0.6	9.80	1	45: 15-19	1.2	9.64	0	70: 22-23	1.2	10	0
20: 8-7	0.9	15.68	0	46: 15-22	1.2	20.63	0	71: 23-14	1.2	9.85	1
21: 8-9	1	10.10	1	47: 16-8	1.5	10.09	1	72: 23-22	1.2	10	0
22: 8-16	1.5	10.09	0	48: 16-10	1.5	10.27	0	73: 23-24	0.6	10.16	0
23: 9-5	1.5	20	0	49: 16-17	0.6	10.46	0	74: 24-13	1.2	11.38	1
24: 9-8	1	10.10	1	50: 16-18	0.9	39.36	1	75: 24-21	0.9	9.77	0
25: 9–10	0.9	27.83	1	51: 17-10	2.1	9.99	0	76: 24-23	0.6	10.16	1
26: 10-9	0.9	27.83	1								

* Free-flow Travel Time (FTT, h), Link Capacity (LC, 10^2veh/h), Candidate Location (CL).

References

Agrawal, S., Zheng, H., Peeta, S., Kumar, A., 2016. Routing aspects of electric vehicle drivers and their effects on network performance. Transp. Res. Part D 46, 246–266.

Ban, J.X., Liu, H.X., Ferris, M.C., Ran, B., 2006. A general MPCC model and its solution algorithm for continuous network design problem. Math. Comput. Model. 43 (5), 493–505.

Biegler, L.T., Zavala, V.M., 2009. Large-scale nonlinear programming using IPOPT: an integrating framework for enterprise-wide dynamic optimization. Comput. Chem. Eng. 33 (3), 575–582.

Boyac, B., Zografos, K.G., Geroliminis, N., 2017. An integrated optimization-simulation framework for vehicle and personnel relocations of electric carsharing systems with reservations. Transp. Res. Part B 95, 214–237. doi:10.1016/j.trb.2016.10.007. http://www.sciencedirect.com/science/article/pii/S0191261515301119

Brandstätter, G., Kahr, M., Leitner, M., 2017. Determining optimal locations for charging stations of electric car-sharing systems under stochastic demand. Transp. Res. Part B 104, 17–35. doi:10.1016/J.TRB.2017.06.009. https://www.sciencedirect.com/science/article/pii/S0191261516308359

Byrd, R.H., Nocedal, J., Waltz, R.A., 2006. Knitro: an integrated package for nonlinear optimization. In: Large-Scale Nonlinear Optimization. Springer, pp. 35–59.

Chang, W.S., Lei, P.Y., Chyu, C.C., 2007. Local-search based metaheuristics for the multi-source capacitated facility location problem. In: International Conference on Information & Management Sciences.

Chen, Z., He, F., Yin, Y., 2016. Optimal deployment of charging lanes for electric vehicles in transportation networks. Transp. Res. Part B 91, 344–365.

Dafermos, S.C., Sparrow, F.T., 1969. The traffic assignment problem for a general network. J. Res. Natl. Bureau Standards B 73 (2), 91–118.

Dirkse, S., Ferris, M., Meeraus, A., 2002. Mathematical Programs with Equilibrium Constraints: Automatic Reformulation and solution via Constraint Optimization, pp. 67–93.

Dong, J., Liu, C., Lin, Z., 2014. Charging infrastructure planning for promoting battery electric vehicles: an activity-based approach using multiday travel data. Transp. Res. Part C 38, 44–55.

Drud, A.S., 1994. CONOPT a large-scale GRG code. ORSA J. Comput. 6 (2), 207–216.

Egbue, O., Long, S., 2012. Barriers to widespread adoption of electric vehicles: an analysis of consumer attitudes and perceptions. Energy Policy 48, 717–729.

Fernandes, D.R., Rocha, C., Aloise, D., Ribeiro, G.M., Santos, E.M., Silva, A., 2014. A simple and effective genetic algorithm for the two-stage capacitated facility location problem. Comput. Ind. Eng. 75, 200–208. doi:10.1016/J.CIE.2014.05.023. https://www.sciencedirect.com/science/article/pii/S0360835214001764

Fletcher, R., Leyffer, S., 2002. Nonlinear programming without a penalty function. Math. Program. 91 (2), 239–269.

Fletcher, R., Leyffer, S., Ralph, D., Scholtes, S., 2006. Local convergence of SQP methods for mathematical programs with equilibrium constraints. SIAM J. Optim. 17 (1), 259–286.

Frade, I., Ribeiro, A., Gonçalves, G., Antunes, A., 2011. Optimal location of charging stations for electric vehicles in a neighborhood in Lisbon, Portugal. Transp. Res. Record (2252) 91–98.

Friesz, T., Bernstein, D., Smith, T., Tobin, R., Wie, B.-W., 1993. A variational inequality formulation of the dynamic network user equilibrium problem. Oper. Res. 41, 179–191. doi:10.1287/opre.41.1.179.

Friesz, T.L., 1985. Transportation network equilibrium, design and aggregation: key developments and research opportunities. Transp. Res. Part A 19 (5), 413–427. doi:10.1016/0191-2607(85)90041-X. Special Issue Transportation Research: The State of the Art and Research Opportunities

Gagarin, A., Corcoran, P., 2018. Multiple domination models for placement of electric vehicle charging stations in road networks. Comput. Oper. Res. 96, 69–79. https://www.sciencedirect.com/science/article/pii/S0305054818300832

Gagarin, A., Corcoran, P., 2018. Multiple domination models for placement of electric vehicle charging stations in road networks. Comput. Oper. Res. 96, 69–79. doi:10.1016/J.COR.2018.03.014.

Green, L.V., Kolesar, P.J., Soares, J., 2001. Improving the sipp approach for staffing service systems that have cyclic demands. Oper. Res. 49 (4), 549–564.

Green, L.V., Soares, J., 2007. Note computing time-dependent waiting time probabilities in M(t)/M/s(t) queuing systems. Manuf. Serv. Oper. Manage. 9 (1), 54–61.

Halper, R., Raghavan, S., Sahin, M., 2015. Local search heuristics for the mobile facility location problem. Comput. Oper. Res. 62, 210–223. doi:10.1016/J.COR.2014.09.004. https://www.sciencedirect.com/science/article/pii/S0305054814002512

Harker, P.T., Pang, J.-S., 1988. Existence of optimal solutions to mathematical programs with equilibrium constraints. Oper. Res. Lett. 7 (2), 61–64.

He, F., Wu, D., Yin, Y., Guan, Y., 2013. Optimal deployment of public charging stations for plug-in hybrid electric vehicles. Transp. Res. Part B 47, 87–101.

He, F., Yin, Y., Lawphongpanich, S., 2014. Network equilibrium models with battery electric vehicles. Transp. Res. Part B 67, 306–319.

He, L., Mak, H.-Y., Rong, Y., Shen, Z.-J.M., 2017. Service region design for urban electric vehicle sharing systems. Manuf. Serv. Oper. Manage. 19 (2), 309–327. doi:10.1287/msom.2016.0611.

He, S.Y., Kuo, Y.-H., Wu, D., 2016. Incorporating institutional and spatial factors in the selection of the optimal locations of public electric vehicle charging facilities: a case study of beijing, china. Transp. Res. Part C 67, 131–148. doi:10.1016/J.TRC.2016.02.003. https://www.sciencedirect.com/science/article/pii/S0968090X16000486

Huntington, H.G., 2010. Short-and long-run adjustments in US petroleum consumption. Energy Econ. 32 (1), 63–72.

Jiang, N., Xie, C., 2014. Computing and analyzing mixed equilibrium network flows with gasoline and electric vehicles. Comput.-Aided Civil Infrastruct. Eng. 29 (8), 626–641.

Jung, J., Chow, J.Y., Jayakrishnan, R., Park, J.Y., 2014. Stochastic dynamic itinerary interception refueling location problem with queue delay for electric taxi charging stations. Transp. Res. Part C 40, 123–142. doi:10.1016/J.TRC.2014.01.008. https://www.sciencedirect.com/science/article/pii/S0968090X14000126

Kang, Q., Wang, J., Zhou, M., Ammari, A.C., 2016. Centralized charging strategy and scheduling algorithm for electric vehicles under a battery swapping scenario. IEEE Trans. Intell. Transp. Syst. 17 (3), 659–669.

Lévay, P.Z., Drossinos, Y., Thiel, C., 2017. The effect of fiscal incentives on market penetration of electric vehicles: a pairwise comparison of total cost of ownership. Energy Policy 105, 524–533.

Leyffer, S., Munson, T., 2010. Solving multi-leader–common-follower games. Optim. Methods Softw. 25 (4), 601–623.

Liu, H., Wang, D.Z., 2017. Locating multiple types of charging facilities for battery electric vehicles. Transp. Res. Part B 103 (Supplement C), 30–55. Green Urban Transportation

Mak, H.-Y., Rong, Y., Shen, Z.-J.M., 2013. Infrastructure planning for electric vehicles with battery swapping. Manage. Sci. 59 (7), 1557–1575.

Muller, J., 2013. Tesla and Nissan: EV battery swap replaces anxiety with peace of mind. https://www.forbes.com/sites/joannmuller/2013/06/21/tesla-and-nissan-ev-battery-swap-replaces-anxiety-with-peace-of-mind/

Nguyen, S., Dupuis, C., 1984. An efficient method for computing traffic equilibria in networks with asymmetric transportation costs. Transp. Sci. 18 (2), 185–202.

Riemann, R., Wang, D.Z., Busch, F., 2015. Optimal location of wireless charging facilities for electric vehicles: flow-capturing location model with stochastic user equilibrium. Transp. Res. Part C 58, 1–12.

Sadeghi-Barzani, P., Rajabi-Ghahnavieh, A., Kazemi-Karegar, H., 2014. Optimal fast charging station placing and sizing. Appl. Energy 125, 289–299.

Scheel, H., Scholtes, S., 2000. Mathematical programs with complementarity constraints: stationarity, optimality, and sensitivity. Math. Oper. Res. 25 (1), 1–22.

Scholtes, S., 2001. Convergence properties of a regularization scheme for mathematical programs with complementarity constraints. SIAM J. Optim. 11 (4), 918–936.

Tran, T.H., Nagy, G., Nguyen, T.B.T., Wassan, N.A., 2018. An efficient heuristic algorithm for the alternative-fuel station location problem. Eur. J. Oper. Res. 269 (1), 159–170. doi:10.1016/J.EJOR.2017.10.012. https://www.sciencedirect.com/science/article/pii/S0377221717309062

Wächter, A., Biegler, L.T., 2006. On the implementation of an interior-point filter line-search algorithm for large-scale nonlinear programming. Math. Program. 106 (1), 25–57.

Widrick, R.S., Nurre, S.G., Robbins, M.J., 2016. Optimal policies for the management of an electric vehicle battery swap station. Transp. Sci..

Worley, O., Klabjan, D., Sweda, T.M., 2012. Simultaneous vehicle routing and charging station siting for commercial electric vehicles. In: Electric Vehicle Conference (IEVC), 2012 IEEE International. IEEE, pp. 1–3.

Wu, F., Sioshansi, R., 2017. A stochastic flow-capturing model to optimize the location of fast-charging stations with uncertain electric vehicle flows. Transp. Res. Part D 53, 354–376. doi:10.1016/J.TRD.2017.04.035. https://www.sciencedirect.com/science/article/pii/S136192091630102X

Xu, M., Meng, Q., Liu, K., 2017. Network user equilibrium problems for the mixed battery electric vehicles and gasoline vehicles subject to battery swapping stations and road grade constraints. Transp. Res. Part B 99, 138–166.

Yang, J., Sun, H., 2015. Battery swap station location-routing problem with capacitated electric vehicles. Comput. Oper. Res. 55, 217–232.